On the Mediterranean Water Composition

L. I. CARRACEDO

*Faculty of Marine Sciences, University of Vigo, Campus Lagoas-Marcosende, and Instituto
de Investigaciones Marinas, CSIC, Vigo, Spain*

P. C. PARDO

Instituto de Investigaciones Marinas, CSIC, Vigo, Spain

S. FLECHA

Instituto de Ciencias Marinas de Andalucía, CSIC, Puerto Real, Cádiz, Spain

F. F. PÉREZ

Instituto de Investigaciones Marinas, CSIC, Vigo, Spain

ABSTRACT

The Mediterranean Outflow Water (MOW) spills from the Mediterranean Sea (east North Atlantic basin) west off the Strait of Gibraltar. As MOW outflows, it entrains eastern North Atlantic Central Waters (ENACW) and Intermediate Waters to form the neutrally buoyant Mediterranean Water (MW) that can be traced over the entire North Atlantic basin. Its high salinity content influences the thermohaline properties of the intermediate–deep water column in the North Atlantic and its dynamics. Here, the composition of MW in its source region (the Gulf of Cádiz, west off Strait of Gibraltar) is investigated on the basis of an optimum multiparameter analysis. The results obtained indicate that mixing of MOW ($34.1\% \pm 0.3\%$) occurs mainly with overlying ENACW ($57.1\% \pm 0.8\%$) in a process broadly known as central water entrainment. A diluted form (80% of dilution) of the Antarctic Intermediate Water (AAIW) reaches the region and also takes part in MW formation ($8.3\% \pm 0.5\%$). Finally, the underlying Labrador Sea Water (LSW) also contributes ($0.4\% \pm 0.1\%$) to the characteristics of MW. From these results and considering 0.74 Sverdrups (Sv; $1\,\mathrm{Sv} \equiv 10^6\,\mathrm{m^3\,s^{-1}}$) as the mean outflow of MOW, the MW exportation rate was inferred (2.2 Sv), which, decomposing MW, means that the MOW outflow is accompanied by 1.24 Sv of entrained ENACW, 0.18 Sv of AAIW, and <0.01 Sv of LSW.

1. Introduction

Mediterranean Water (MW) provides the North Atlantic basin with unique thermohaline properties. Its salinity maximum can be clearly traced in the entire North Atlantic (Reid 1994), and it has been the subject of numerous studies (Arhan and King 1995; Iorga and Lozier 1999a,b; van Aken 2000b). MW transfers some thermohaline signature to the lower meridional overturning circulation limb by means of the North Atlantic Deep Water formation (Reid 1994), and therefore it plays a notable role on the meridional overturning circulation and, by extension, in the large-scale climate (Lionello et al. 2006). Also significant, MW is the water mass with the highest lead content (Malakoff 2014), thus printing and extending a traceable signal of pollution from the Mediterranean Sea into the North Atlantic. MW originates in the Gulf of Cádiz (GoC), a region south of the Iberian Peninsula (from the Strait of Gibraltar until approximately 7°W; Fig. 1), by mixing of the outflow from the Mediterranean Sea [Mediterranean Outflow Water (MOW)] with the subsurface and intermediate waters of the northeast Atlantic basin (Worthington 1976; Baringer and Price 1997).

Corresponding author address: Lidia Isabel Carracedo Segade, Physical Oceanography Group (GOFUVI), Department of Applied Physics, Faculty of Marine Sciences, University of Vigo (Spain), Campus Lagoas-Marcosende, 36200, Vigo, Spain.
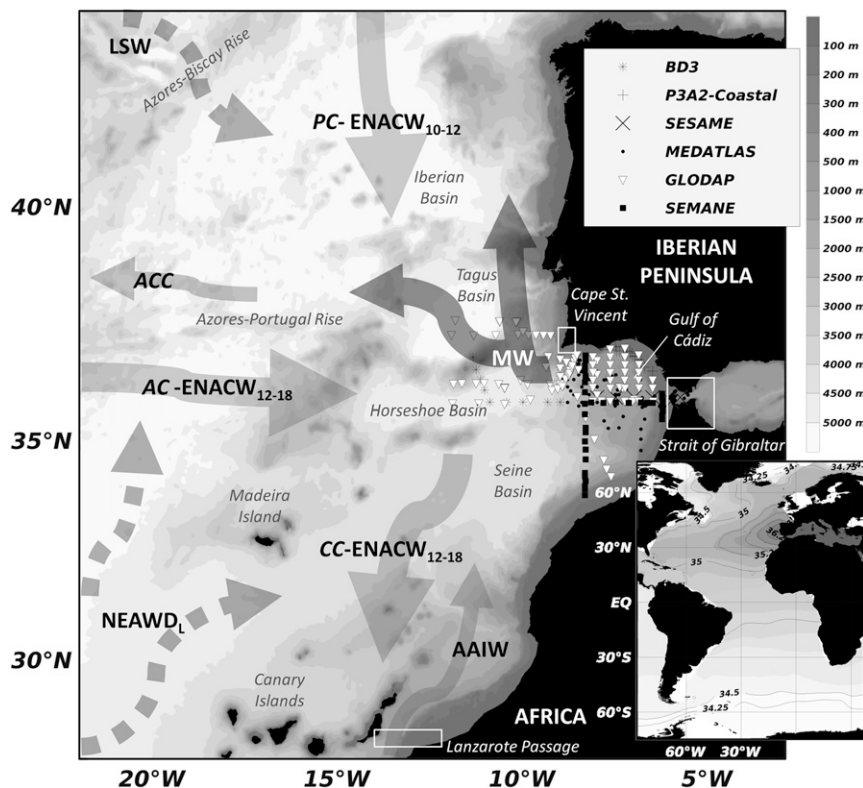E-mail: lcarracedo@uvigo.es

FIG. 1. Location of the station data used in this study (see Table 1 for reference). Shaded arrows roughly indicate main currents and water masses advective paths: Portugal Current (PC), Azores Current (AC), Azores Counter Current (ACC), Canary Current (CC), ENACW (18°, 12°, and 10°C), MW, AAIW, LSW, and NEADW$_L$. Inset map shows the salinity contours [*World Ocean Atlas 2009* (*WOA09*); psu] on the $\sigma_1 = 32.2 \, \mu\text{mol kg}^{-1}$ (σ_1; potential density referred to 1000 dbar).

The Mediterranean Sea is a semienclosed sea located on the eastern side of the North Atlantic basin (Fig. 1), and it is characterized by a two-layer thermohaline cell of circulation with an order of magnitude of 1 Sverdrup (Sv; 1 Sv $\equiv$ $10^6 \, \text{m}^3 \, \text{s}^{-1}$) (Lionello et al. 2006). Atlantic Water—mean value of the salinity minimum at the Strait of Gibraltar of $S = 36.2$ psu (García-Lafuente et al. 2007, 2011)—inflows through the Strait of Gibraltar (Fig. 1) in the upper layer toward the Mediterranean Sea. As it spreads eastward, its salinity (and consequently its density) increases through intense evaporation. During winter, the cooling increases its density even more and favors the water mass sinking by deep convection. This newly formed water mass spreads back to the west at intermediate levels, mixing on the way with the surrounding waters, and reaches the Strait of Gibraltar as MOW (Zenk 1975; Rhein and Hinrichsen 1993; Baringer and Price 1997; Siedler et al. 2001; Huertas et al. 2012).

After leaving the Strait of Gibraltar, MOW ($S = 38.402$– 38.408 psu and $\theta = 13.145°$C; García-Lafuente et al. 2007, 2011) spills over the slope, dragging and entraining eastern North Atlantic Central Water (ENACW; Zenk and Armi 1990; Price et al. 1993; Rhein and Hinrichsen 1993). This process of downwelling and mixing generates an area of convergence and subduction (overturning circulation) in the GoC that will have a dynamical impact on the upper-layer circulation of the subtropical eastern North Atlantic (Jia 2000).

As a result of the mixing undergone, the MOW volume increases more than twice [from 1 to 3 Sv, according to Worthington (1976), or from 0.7 to 1.9 Sv, according to Baringer and Price (1997)], and the result is a less saline water mass, which we will particularly refer to as MW (Ríos et al. 1992; Ambar et al. 1999; van Aken 2000b; Àlvarez et al. 2004, 2005; Fusco et al. 2008; Alves et al. 2011). With MOW being the origin of MW and the real input from the Mediterranean Sea, MW will become a well-differentiated neutrally buoyant water body that will spread from the Cape St. Vincent (Fig. 1) into the entire North Atlantic.

In the GoC, until approximately 7°W, MW is still a bottom-trapped density current (Baringer and Price 1997). By about 7.5°W, the deeper portion of the MW starts to detach from the bottom and begins to intrude into the North Atlantic thermocline. Once the flow reaches Cape St. Vincent (Fig. 1), it becomes neutrally buoyant and

floats off the bottom (Baringer and Price 1997, 1999). MW flows mainly northward along the European western margin, parallel to the bathymetry contours until the Porcupine Bank (53°N). It also follows a westward/southwestward route mostly associated with the movement of intermediate anticyclonic eddies (meddies; Bower et al. 1995; Shapiro and Meschanov 1996; van Aken 2000b). A less pure core than that of the MW northward vein or meddies also spreads westward (Fig. 1), within a secondary advective route related to the Azores Countercurrent (Carracedo et al. 2014, 2015).

The relevance of the contribution of MW on intermediate–deep layers of the North Atlantic circulation has been noticed (Reid 1978, 1979, 1994; Saunders 1982; Emery and Meincke 1986; Arhan 1987; Schmitz 1996) and considered in previous studies intending to quantify the water masses mixing in this region of the ocean (Álvarez et al. 2004, 2005; Louarn and Morin 2011; Carracedo et al. 2012, 2014, 2015). All these latter studies have made use of optimum multiparameter (OMP) analyses (Tomczak 1981; Tomczak and Large 1989), which are relatively simple mathematical approaches to solve the water mass structure. In particular, the composition of the MW has been investigated in various previous studies. Zenk (1975) estimated MW as the mixing between MOW and North Atlantic Central Waters (32% and 68%, respectively, based on temperature and salinity). Lately in a deeper study, Rhein and Hinrichsen (1993) investigated the contribution of MOW and central waters to the double maximum feature of MW (Zenk 1970, 1975; Howe et al. 1974; Ambar and Howe 1979a; Zenk and Armi 1990). They found a higher in situ nutrient concentration than expected by ENACW–MW mixing, which was attributed to the possible local nutrient sources in the Gulf. As a response to these latter result, Louarn and Morin (2011) outlined the possible implication of the Antarctic Intermediate Water (AAIW) in the formation of MW, thereby making Rhein and Hinrichsen's hypothesis of an external nutrient source no longer necessary. Louarn and Morin (2011) quantified the proportion of AAIW in the MW by using a highly diluted local form ($\theta = 10.254°C$; $S = 35.623$ psu).

Considering the potential influence that the Mediterranean Sea and its variability may have on the dynamical scenario of the North Atlantic circulation, it can be an advantage for future water mass studies to consider the signal of MW from its original sources. This study provides new and robust estimates of the composition of MW (i.e., the ratio between MW source water masses), as well as a more general view of the mixing between the water masses characterizing the GoC region (Fig. 1). We have used historical data in order to obtain a more extended sampled area with respect to previous studies. Besides, we have developed an OMP analysis based on more general definitions of the water masses and for the whole water column in order to have a clear vision of the water mass interaction in the GoC. In the analysis, the main subtropical and subpolar varieties of the ENACW are considered separately and the influence of the deep and bottom North Atlantic waters is also taken into account. Here, we consider the characteristics of the AAIW core flowing in the eastern North Atlantic as it passes through the Lanzarote Passage on its way northward (Fig. 1), which is the location that provides the most complete and reliable AAIW characterization in the eastern North Atlantic at these latitudes (Machín and Pelegrí 2009). The characteristics of the resulting MW define the main core, which enters the circulation system of the North Atlantic region. Our results tend to be concordant with the water mass transports assigned to the MW flow into the North Atlantic.

The paper is organized as follows: In section 2, we describe the data used in the study (section 2a), the methodology followed for the OMP analysis (section 2b), including a description of the water masses participating, the variables included, and how we model their mixing and the methodology followed to provide the MW decomposition. In section 3, we describe and discuss the results from the OMP analysis (contributions to the mixing of the different water masses; section 3a) and the decomposition of MW in its source water masses (section 3b). And finally, in section 4, we resume the results and conclude the study.

2. Data and method

a. Dataset

We have compiled historical data in the GoC region (Fig. 1) that covered this area from 34° to 37°N in latitude and from 5.5° to 9°W in longitude. The dataset (Table 1) was constructed by means of two databases and seven particular cruises. The hydrographic cruises included in the dataset were Bord-Est 3 (DB3-1989; Fig. 1, asterisks), Sortie des Eaux Méditerranéennes en Atlantique Nord-Est (SEMANE-2002; Fig. 1, squares), Producción Pelágica en la Plataforma Atlántico-Andaluza (P3A2-2007; Fig. 1, plus signs), and two last cruises from the Southern European Seas: Assessing and Modeling Ecosystem Changes (SESAME-2008) project (Fig. 1, crosses). Regarding the databases, we took only those data having all the variables needed for the OMP analysis [see appendix A]. Two databases were used: the Global Ocean Data Analysis Project (GLODAP; http://cdiac.ornl.gov/oceans/glodap/), where we obtained data

TABLE 1. Summary of data combined to construct the Gulf of Cadiz OMP database.

Data		Date		No. stations	No. bottle data	References
Databases	MEDATLAS	1948	to 1998	71	790	Fusco et al. (2008)
	GLODAP	1981	to 2013	87	1185	
Additional Cruises	BD3	9 May 1989	26 May 1789	13	160	
	SEMANE	16 Jul 2002	22 Jul 2002	37	331	Louarn and Morin (2011); Alves et al. (2011)
	P3A2-COASTAL	13 Oct 2007	23 Oct 2007	14	15	
	SESAME I–II	13 Apr 2008	14 Apr 2008	6	25	Huertas et al. (2012)
		25 Sep 2008	27 Sep 2008	6	38	
			Total data	311	3174	

from 1981 to 2013, and the Mediterranean Data Archaeology and Rescue (MEDAR)/Mediterranean Hydrographic Atlas (MEDATLAS; http://www.ifremer.fr/medar/), where we selected data from 1998 to 2001.

b. Multiparameter mixing (OMP) analysis

The main principle behind the OMP analyses (Tomczak 1981) is to consider the physical and chemical properties, measured at each single point in the ocean, to be the result of the mixing of a certain number of water masses [source water types (SWTs)] present in the region. From their beginning, the OMP analysis have been widely used in oceanography and not only to study the water masses structure and mixing (Castro et al. 1998; Poole and Tomczak 1999; Álvarez et al. 2004, 2005, 2014; Johnson 2008; Louarn and Morin 2011; Pardo et al. 2012) and/or their temporal variability (Carracedo et al. 2012; García-Ibáñez et al. 2015), but also to solve nutrient mineralization and oxygen utilization patterns (Pérez et al. 1993, 1998, 2001; Lønborg and Álvarez-Salgado 2014; Álvarez-Salgado et al. 2014), the age of the water masses (Karstensen and Tomczak 1997), or the anthropogenic carbon storage in the ocean (Álvarez et al. 2004, 2005; Flecha et al. 2012; Pardo et al. 2012).

In mathematical terms, the OMP analysis is a mathematical approach based on measured data that solves the mixing between SWTs by a least squares method constrained to be positive definite. The SWTs are points in the n-dimensional parameter space (with n as the number of properties that characterize each SWT) and refers to a water body used as reference, either corresponding to a water mass originally formed at its source region by air–sea interaction or to a variety of it. SWTs' physicochemical characteristics are supposed to be well known, constant with time, and equally affected by mixing. Directly related to this latter assumption, those layers of the water column affected by air–sea interaction are excluded from the analysis (broadly first 50 dbar). Because of the

assumption of time invariance of the SWTs' properties, the distribution of the SWTs may also reflect, in addition to the spatial variability of their spreading, the interannual variations of the pure SWTs during their formation. As result, the fractions X_i of a specific subset of i SWTs (mixed by diapycnal or isopycnal mixing processes) are obtained from the characteristics of a given water sample. The different subsets of SWTs involved in a mixing process are what we will refer to as mixing figures (MFs). The term figure refers to the geometrical space in the θ–S plane formed by two SWTs (line segment), three SWTs (triangle), four SWTs (square), and so on. Actually, the mixing figures are n-dimensional spaces. In this study, each mixing figure was constituted by a maximum of four SWTs in order to solve the system of seven equations (appendix A; Table A1) and five unknowns (X_1, X_2, X_3, X_4, and ΔO; with ΔO as the oxygen consumed in the sample due to the respiration of organic matter) with at least two degrees of freedom (i.e., number of unknowns < number of equations).

The choice of the MFs will be based on the following aspects: (i) the characteristics and vertical distribution of the water masses, (ii) the dynamics of the SWTs in the region of study, and (iii) the continuity of the mixing by imposing that each MF has at least two SWTs in common with the neighboring MF. For a given sample, the MF whose fractions X_i reproduce the best the properties (produce the lowest residual) will be assigned to this sample on the basis of an OMP analysis using only conservative variables [for more information see the works by Pardo et al. (2012) and García-Ibáñez et al. (2015)].

Here, we make use of a (two step) methodology [section 2b(2)] based on OMP analyses in order to obtain the fractions of eight SWTs characterizing the GoC. Of relevance for the eOMP setup, we will first describe [section 2b(1); Table 2] the main water masses in the region of study and their definitions (SWTs).

TABLE 2. Summary and references for the main Source Water Types (SWTs) found in the Gulf of Cádiz region.

	Name	Acronym	Characteristics	References
Central	Eastern North Atlantic Central Water Subtropical	ENACW$_{18}$	Warmest subtropical central mode water found in the area of study, originally formed at the northern margin of the Azores Current (ENACW$_{16}$) at about 36°N and modified a posteriori by air–sea interaction	Gascard and Richez (1985); Ríos et al. (1992); Criado-Aldeanueva et al. (2006)
	Eastern North Atlantic Central Water of Harvey	ENACW$_{12}$	Limit between subpolar and subtropical modes	Harvey (1982); Ríos et al. (1992); Castro et al. (1998)
	Eastern North Atlantic Central Water Subpolar	ENACW$_{10}$	Coldest central mode water originally formed at the cyclonic gyre located in the northeast Atlantic	Harvey (1982); Fiúza et al. (1998)
Intermediate	Mediterranean Outflow Water	MOW	Saltiest water spilling down across the Strait of Gibraltar originally formed in the Mediterranean Sea	Reid (1994); García-Lafuente et al. (2007)
	Mediterranean Water	MW	Characterized by a salinity maximum, water mass formed in the Gulf of Cádiz region by entrainment of central waters to the MOW	Ambar and Howe (1979a); Price et al. (1993); Pérez et al. (2001); Álvarez et al. (2005)
	Antarctic Intermediate Water	AAIW	Originally formed in the Antarctic Subpolar Front, is characterized by a salinity minimum and silicate maximum	Tsuchiya (1989); Talley (1996); Machín and Pelegrí (2009)
Deep	Labrador Sea Water	LSW	Originally formed in the Labrador Sea, is characterized by an oxygen maximum	Paillet et al. (1998)
Bottom	Northeast Atlantic Deep Water lower	NEADW$_L$	Remains of the Antarctic Bottom Water that enters the eastern Atlantic basins at the Vema Fracture Zone near 10°N. Characterized by a silicate maximum	Harvey (1982); Saunders (1982)

1) θ–S DIAGRAM AND WATER MASSES CHARACTERIZATION

In the eastern North Atlantic, the central waters (ENACW) are characterized by a θ–S mixing line that can be split into two segments (Fig. 2) that represent the subtropical and the subpolar branches (Ríos et al. 1992). The inflection point (ENACW$_{12}$, 12.2°–12.30°C, 35.66 psu; Castro et al. 1998) between both segments is the upper limit of the subpolar ENACW given by Harvey (1982). Originally the Subtropical Mode Water is formed at the northern margin of the Azores Current (around 36°N; Fig. 1) spreading toward the Iberian Peninsula (Ríos et al. 1992) and reaching the GoC region. Because its properties vary mainly due to air–sea interactions (Pollard and Pu 1985), here we will refer to this uppermost ENACW extreme as ENACW$_{18}$, characterizing the upper layers of the GoC region with a straight line (ENACW$_{12}$ to ENACW$_{18}$) in the θ–S diagram (Fig. 2; Gascard and Richez 1985; Criado-Aldeanueva et al. 2006). As for the lowest ENACW bound, ENACW$_{10}$

accounts for the Subpolar Mode Water that is originally formed at high latitudes in the Subpolar Gyre by winter convection, commonly known in that source region as Subpolar Mode Water (8.0°C, 35.23 psu; McCartney and Talley 1982; Brambilla and Talley 2008). At lower latitudes, the presence of this water mass likely relates to the southward recirculation of the North Atlantic Current in the eastern basin. A pronounced southward subduction extension of Subpolar Mode Water is depicted (Paillet and Arhan 1996), ventilating the permanent thermocline at those latitudes (Keffer 1985). Off the Portuguese coast, and as we get closer to the GoC region, the mixing with the underlying MW (van Aken 2000b) abruptly erodes the Subpolar Mode Water θ–S extreme (Emery and Meincke 1986). We resorted to water mass studies off the Iberian coast (Fig. 1; Harvey 1982; Fiúza et al. 1998), whose definition, from in situ data, coincided with the lower limit of the deeper ENACW straight segment (10.0°C, 35.40 psu), that is, ENACW$_{10}$.

The overflow from the Mediterranean Sea stays below the central waters. MOW properties (13.2°C, 38.4 psu; Fig. 2) were selected as the extreme properties of the
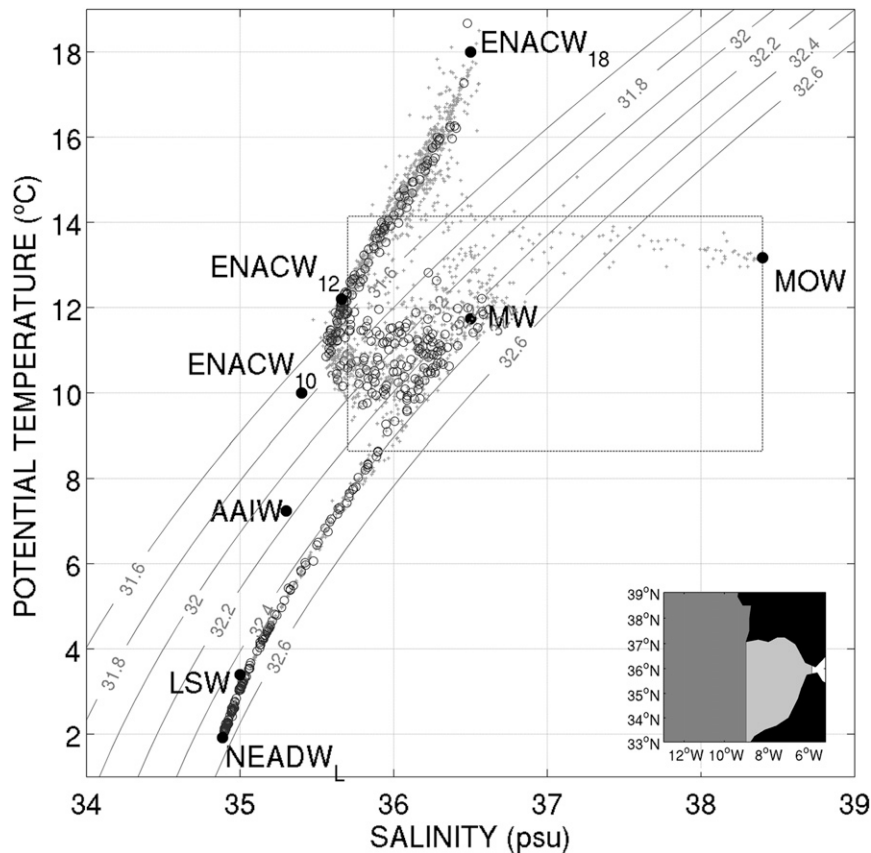
FIG. 2. Potential temperature (θ, surface reference level) vs salinity diagram showing the position of the source water types. Dark (light) gray circles (crosses) correspond to data west (east) Cape St. Vincent. Inlet figure shows in dark (light) gray, the area for which data are shown. Gray lines correspond to σ_1 isopycnals. East North Atlantic Central Water (ENACW$_\theta$; with $\theta = 18°$, $12°$, or $10°C$), MW, MOW, AAIW, LSW, and NEADW$_L$. The dotted square comprises data used in section 3a(2).

overflow in the Strait of Gibraltar, at Camarinal Sill (5.75°W; Gascard and Richez 1985; Rhein and Hinrichsen 1993; Reid 1994; García-Lafuente et al. 2007). Once MOW reaches the GoC it mixes with central and intermediate waters forming MW. Actually, the mixing process between MOW and the surrounding waters in the GoC region leads to the formation of two cores of MW at different depths: intermediate (~800 m) and deep (~1200 m; Howe et al. 1974; Zenk 1975; Ambar and Howe 1979a; Baringer and Price 1997; Iorga and Lozier 1999a,b). Moreover, some studies have identified a very local presence of a shallower subsurface core (~400 m; Madelain 1970; Ambar 1983). At 20°W generally the intermediate core is no longer distinguishable (Tsuchiya et al. 1992) so that the deep MW core will be the diffuse Mediterranean "tongue" spreading, at about 1200-m depth, through the entire North Atlantic, mixing with the surrounding waters and modifying mostly the salinity of intermediate-to-deep

waters in the North Atlantic basin (Talley 1996). In the northeast Atlantic, the typical properties for MW (11.74°C; 36.5 psu; Fig. 2) correspond to that deeper core once stabilized at 9°W (Ambar and Howe 1979a; Price et al. 1993; Pérez et al. 2001; Álvarez et al. 2004, 2005). In this study, we are interested in this more general understanding of MW, rather than differentiating between cores, in order to provide a simplified relation between the Mediterranean Sea and the North Atlantic water masses' contributions. Note, in that case, that the upper core of MW will be understood as a continually decreasing contribution of MW upward from its deepest core with extreme thermohaline properties.

AAIW forms in southern polar regions ($3.14° < \theta < 5.6°C$, $34.14 < S < 34.4$ psu; McCartney and Talley 1982), near the Subantarctic Front (Tsuchiya 1989; Talley 1996), and flows northward in the Atlantic Ocean mainly through the western boundary current system and its eastward extensions (Tomczak and Hughes 1980;

TABLE 3. Characteristics of SWTs with their correspondent STD, the square of correlation coefficients (r^2, values expressed on a per one basis) of the regression between the measured (samples) and predicted variables (obtained substituting X_i in the equations), the SDR, the accuracies of the measured properties (ε), and the SDR/ε ratios from the data below 400 dbar. Note O_2^0 concentrations represent close to saturation values (saturation values in parentheses) and nutrients are those recomputed after iteration (departure values in parentheses). O_2 and nutrients represent preformed values (superscript 0).

	θ (°C)	S (psu)	O_2^0 (μmol kg^{-1})	SiO_2^0 (μmol kg^{-1})	NO_3^0 (μmol kg^{-1})	PO_4^0 (μmol kg^{-1})
ENACW$_{18}$	18.0 ± 0.4	36.50 ± 0.02	250 (250) ± 3	0.0 (0.0) ± 0.1	0.0 (0.0) ± 0.1	0.00 (0.00) ± 0.01
ENACW$_{12}$	12.20 ± 0.4	35.66 ± 0.02	256 (261) ± 3	3.81 (4.00) ± 0.08	5.7 (6.1) ± 0.1	0.30 (0.31) ± 0.01
ENACW$_{10}$	10.0 ± 0.3	35.40 ± 0.01	185 (274) ± 3	6.6 (6.6) ± 0.1	17.2 (17.8) ± 0.4	1.06 (0.92) ± 0.02
MOW	13.17 ± 0.03	38.40 ± 0.01	181 (251) ± 3	8.0 (7.9) ± 0.4	8.3 (9.36) ± 0.7	0.43 (0.49) ± 0.07
AAIW	7.24 ± 0.1	35.30 ± 0.02	160 (291) ± 3	19.5 (19.5) ± 0.4	28.6 (28.7) ± 0.9	1.72 (1.75) ± 0.05
LSW	3.40 ± 0.2	35.00 ± 0.12	255 (319) ± 3	16.5 (17.7) ± 0.4	18.6 (20.1) ± 0.5	1.22 (1.37) ± 0.03
NEADW$_L$	1.92 ± 0.03	34.885 ± 0.003	248 (332) ± 3	47.8 (47.0) ± 1	21.5 (20.5) ± 0.5	1.50 (1.39) ± 0.03
r^2	0.9996	0.995	0.98	0.9925	0.96	0.96
SDR	0.04	0.01	2.7	0.6	1.0	0.06
ε	0.005	0.005	3.3	0.5	0.2	0.002
SDR/ε	10	7	1	2	6	4

Reid 1994). It has been identified as far as 32°N in the eastern North Atlantic basin (van Aken 2000a; Álvarez et al. 2005). Despite the erosion while it spreads, AAIW is commonly characterized by a salinity minimum and, north of 20°S, by a silicate maximum. Typical thermohaline values given to this water mass in the North Atlantic are in the ranges $6 < \theta < 7.9$°C, and $34.9 < S < 35.0$ psu (Tsuchiya et al. 1992; Pérez et al. 2001; Álvarez et al. 2004, 2005; Carracedo et al. 2012, 2014, 2015). West off the Iberian Peninsula, the presence of MW affects abruptly its salinity minimum. Machín et al. (2006, 2010) and Machín and Pelegrí (2009) have identified and extensively characterized the passage of AAIW ($7° \le \theta \le 8$°C, $S < 35.4$ psu, and $SiO_2 > 15 \mu$mol kg^{-1}) between the Canary Islands and the African coast (Lanzarote Passage; Fig. 1). They set this channel as the main path for AAIW penetration along the North Atlantic eastern margin, that is, the exact location where its extreme properties are found. Here, the θ–S properties of AAIW (Fig. 2) were selected as obtained from the 2009 Shelf–Ocean Exchanges in the Canaries-Iberian Large Marine Ecosystem (CAIBEX) Project Boxlike cruise (CAIBOX-2009) data in the Lanzarote Passage (7.24°C; 35.3 psu; Carracedo et al. 2015).

Finally, the deep to bottom layers of the domain (western half region, from ~1500 m down) are characterized by the presence of the relatively high ventilated (high oxygen) Labrador Sea Water (LSW) and the underlying Northeast Atlantic Deep Water (NEADW). LSW flows anticyclonically into the eastern basin (Paillet and Mercier 1997). To define the SWT for LSW, we have considered the θ–S properties (3.4°C, 34.89 psu) widely accepted for LSW once it crossed the Mid-Atlantic Ridge (Álvarez et al. 2005) but slightly adjusting the salinity to 35.0 psu, a value that is characteristic for the LSW at the Azores–Biscay Rise (Fig. 1; Paillet

et al. 1998). As for the NEADW, this water mass initially originates in the subpolar region as a result of different entrainments that occur along the journey of the Iceland–Scotland Overflow Water through the Iceland basin (van Aken 2000a). On its way southward through the northeast Atlantic basin, NEADW recirculates anticyclonically in the Iberian basin (Paillet et al. 1998), being influenced by LSW and MW on its upper bound (Dickson and Brown 1994; van Aken 2000a) and by the low salinity, high silica Antarctic Bottom Water of southern origin on its deepest bound (van Aken 2000b). We will refer to this modified AABW SWT as lower NEADW (NEADW$_L$), defined in the eastern basin by the point 1.92°C, 34.89 psu (Fig. 2) following Castro et al. (1998). Those properties correspond to the NEADW$_L$ flowing north across the Vema Fracture Zone (McCartney et al. 1991). NEADW$_L$ circulates strongly constrained by the topography, forming a cyclonic gyre in the eastern basin (Paillet and Mercier 1997). From about 3000 dbar to the bottom, there is a practically linear θ–S relationship for the NEADW (Saunders 1982).

Once the most suitable θ and S properties were defined (Table 3), the chemical characterization of the SWT was completed with their oxygen (O_2^0) and nutrients (NO_3^0, PO_4^0, and SiO_2^0) concentration values (the superscript 0 means preformed variables). The O_2^0 values were initially established equal to saturation (Table 3, in parentheses; Weiss 1970) and then adjusted so as not to get negative values for respiration ($\Delta O \ge 0$) and to account for the disequilibrium between the O_2 content in the atmosphere and in the water mass at its time of formation (in the surface ocean; Ito et al. 2004). In the case of nutrients (Table 3, in parentheses), for ENAWC$_{18}$ they were initially (preiteration values) settled at 0. For ENAWC$_{12}$, ENACW$_{10}$, MOW, and LSW, we based our initial selection on literature [ENAWC$_{12}$

from Carracedo et al. (2012); ENACW$_{10}$, MOW, and LSW from Louarn and Morin (2011)]. Finally, for AAIW the selected chemical properties (O$_2^0$, NO$_3^0$, PO$_4^0$, and SiO$_2^0$) were defined at the same location, and from the same in situ data, as θ–S values [Lanzarote Passage, CAIBOX-2009 cruise; Carracedo et al. (2015) in agreement with Machín et al. (2006, 2010)]. The final chemical properties (SiO$_2^0$, NO$_3^0$, and PO$_4^0$; Table 3) for each SWT are obtained by means of an iterative procedure, which reconstructs the nutrients' values from the water masses' contributions (see appendix A).

The standard deviation (STD) of the SWTs properties (Table 3) were taken from different sources. The θ and S STDs values were all taken from Álvarez et al. (2005) except for NEADW$_L$ (García-Ibáñez et al. 2015) and MOW (in situ data of Huertas et al. 2012). We set the STDs for the nutrients and oxygen as a value equal to 2% and 1% of the preformed value, respectively, since when a water mass is formed the content of O$_2$ is not exactly the saturation value (Ito et al. 2004). STDs are used to perform a perturbation analysis of uncertainties (appendix B) that tests the robustness of the eOMP analysis.

2) OMP AND MEDITERRANEAN WATER DECOMPOSITION METHODOLOGY

To obtain the MW composition, the methodology was divided in two steps of increasing complexity. We first focused on applying the eOMP analysis with the most simplified setup so that we could obtain a first guess of the MW SWT definition. In the second step, we aimed to solve the water masses mixing, including all the end members present in the entire domain of study.

(i) First step

As the very first approximation to the mixing process affecting the MW formation, we limited the domain (by latitude, longitude, and depth) on which we applied the eOMP analysis. For this first guess, we limited the input data to the northern part of the GoC (between 35.5° and 37°N, east of 9°W) and above 1500 dbar. Taking into account the thermohaline characteristics of this specific region, we selected three predefined mixing figures (see polygons in Fig. 3a) that will model the mixing of the six SWTs characterizing this region: 1) [ENACW$_{18}$–ENACW$_{12}$–ENACW$_{10}$–MOW]; 2) [ENACW$_{12}$–ENACW$_{10}$–AAIW–MOW], and 3) [ENACW$_{12}$–ENACW$_{10}$–MOW–LSW].

After applying the OMP analysis and in order to quantify and identify the different sources that compose MW, we delimited a θ–S interval around the θ–S MW core traditionally found in literature (11.74°C; 36.5 psu; Ambar and Howe 1979a; Price et al. 1993; Pérez et al. 2001; Álvarez et al. 2004, 2005). We chose the ±0.5°C and ±0.15-psu ranges, trying to encompass the thermohaline
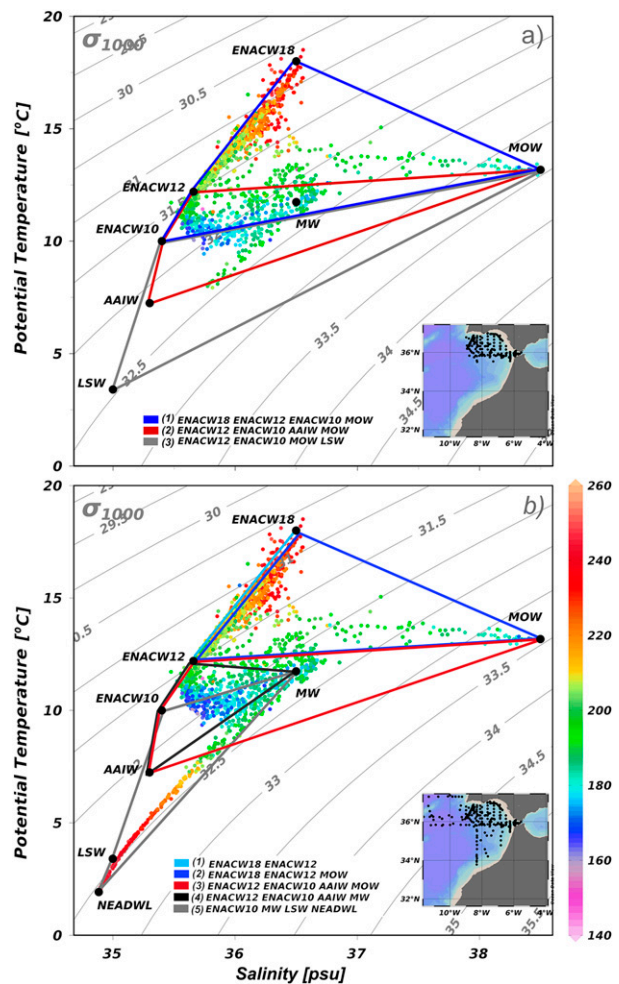

FIG. 3. Potential temperature θ (surface reference level) vs salinity diagram showing the MFs. Black dots mark the position of the SWTs, and polygons show the MFs selected a priori for the OMP analysis. (a) MFs selected for the first step of the methodology (data north of 35.5°N, east of 9°W and shallower than 1500 dbar); (b) MFs selected for the second step of the methodology. Color legend for dots (field data) shows the oxygen concentration (μmol kg^{-1}).

variability reported for this water mass in the last decades (Fusco et al. 2008). We averaged the contributions of all water masses involved in that thermohaline square in order to obtain a first guess of the MW SWT properties:

$$
\begin{aligned}
\text{SWT}_{\text{MW}} = {} & \text{SWT}_{\text{ENACW}_{12}} \times \overline{X}_{\text{ENACW}_{12}} + \text{SWT}_{\text{ENACW}_{10}} \\
& \times \overline{X}_{\text{ENACW}_{10}} + \text{SWT}_{\text{MOW}} \times \overline{X}_{\text{MOW}} \\
& + \text{SWT}_{\text{AAIW}} \times \overline{X}_{\text{AAIW}} + \text{SWT}_{\text{LSW}} \times \overline{X}_{\text{LSW}},
\end{aligned}
\tag{1}
$$

where SWTi refers to the array of SWTs' properties of the water mass i, and $\overline{X}_i$ refers to the mean contribution

TABLE 4. MW properties and standard deviations (when available) from previous works and in this study. In this study, the SWT characteristics correspond to the estimate from the source water masses that lead to MW (in parentheses are preliminary values as result of the first-step estimates; see text).

θ (°C)	S (psu)	O$_2$ (μmol kg^{-1})	SiO$_2$ (μmol kg^{-1})	NO$_3$ (μmol kg^{-1})	PO$_4$ (μmol kg^{-1})	References
36.50	11.74	145 ± 6	11.3 ± 0.9	17.1 ± 0.6	1.04 ± 0.06	Castro et al. (1998)
36.500	11.74	192 ± 4	7.2 ± 0.7	11.9 ± 0.6	0.67 ± 0.04	Pérez et al. (2001)
11.74 ± 0.10	36.50 ± 0.017	263 ± 2	8.6 ± 1	7.1 ± 0.4	0.36 ± 0.05	Álvarez et al. (2004)
11.74 ± 0.1	36.50 ± 0.01	262 ± 5	8.62 ± 0.8	5.16 ± 0.8	0.31 ± 0.1	Álvarez et al. (2005)
11.7 ± 0.1	36.50 ± 0.01	262 ± 5	—	4.0 ± 0.4	0.31 ± 0.08	Lønborg and Álvarez-Salgado (2014)
12.12 ± 0.14	36.68 ± 0.08	188 ± 4	7.36 ± 0.54	12.82 ± 0.5	0.68 ± 0.03	Louarn and Morin (2011)
11.7 ± 0.2	36.500 ± 0.011	210 ± 8	4.88 ± 0.15	10.9 ± 0.2	0.70 ± 0.03	García-Ibáñez et al. (2015)
11.81 (11.73) ± 0.2 (0.30)	36.53 (36.53) ± 0.07 (0.08)	213 (221) ± 7 (9)	7.0 (7.22) ± 0.6 (0.88)	9.9 (9.1) ± 1.1 (1.3)	0.56 (0.51) ± 0.07 (0.08)	This study

of the water mass *i* within the defined θ–S interval. The reconstructed MW SWT was as follows: $\theta = 11.73° \pm 0.30°$C, $S = 36.53 \pm 0.08$ psu, O$_2$ = 220 ± 9, SiO$_2$ = 7.10 ± 0.88, NO$_3$ = 9.1 ± 1.3, and PO$_4$ = 0.51 ± 0.08 μmol kg^{-1}. The θ–S properties are consistent, within their STDs, with the MW SWT used in previous studies (Table 4).

(ii) Second step

Once MW becomes a well-defined water mass body, it directly mixes with surrounding waters. So in order to solve the mixing throughout the whole region of study (all data points available) and to obtain better adjusted and more robust results, we introduced a second step in the methodology. We rerun the procedure, as in step one, but this time using MW as an independent end member (SWT) in the analysis. For the MW SWT thermohaline properties, we kept those broadly accepted in the literature (11.74°C; 36.5 psu; Table 4), and for the chemical properties we used those of the first-step estimate (Table 4). Thermohaline and chemical properties for all the other SWTs were taken the same as the initial setup (Table 3).

This time considering all the domain in study and a total of eight SWTs characterizing the region, we solved the mixing by means of five predefined MFs (see line/polygons in Fig. 3b): 1) [ENACW$_{18}$–ENACW$_{12}$], 2) [ENACW$_{18}$–ENACW$_{12}$–MOW], 3) [ENACW$_{12}$–ENACW$_{10}$–AAIW–MOW], 4) [ENACW$_{12}$–ENACW$_{10}$–AAIW–MW], and 5) [ENACW$_{10}$–MW–LSW–NEADW$_L$]. Note that MFs 3 and 4, are equivalent but changing the Mediterranean origin end member from MOW to MW. On the basis of the robust assumption that all MOW-to-MW transformation takes place east of Cape St. Vincent (Gulf of Cadiz domain), and having done a profile-by-profile θ–S evaluation to validate that assumption, MFs 2 and 3 were geographically constrained to the east of Cape St. Vincent (east of 9°W; Fig. 1). In MF 5, MW was introduced as the only Mediterranean origin end member (not MOW) because it is assumed that below 1000 dbar the mixing with NEADW$_L$ only takes place with water already transformed into MW.

Again, once the OMP analysis was performed, we repeated the procedure to obtain the MW decomposition, delimiting the θ–S interval around the θ–S MW SWT (11.74° ± 0.5°C, 36.5 ± 0.15 psu; Fig. 4). To compute the final MW SWT composition, we considered all points available (samples) within this thermohaline domain (Fig. 4, black squares). Those points within MFs 4 and 5, that is, those points with MW contribution (whose contribution ranges between 85% to 100%; Fig. 4d), were reconverted into its main end members according to $\overline{X}_i^{MF3} \times X_{MW}$, with $\overline{X}_i^{MF3}$ as the
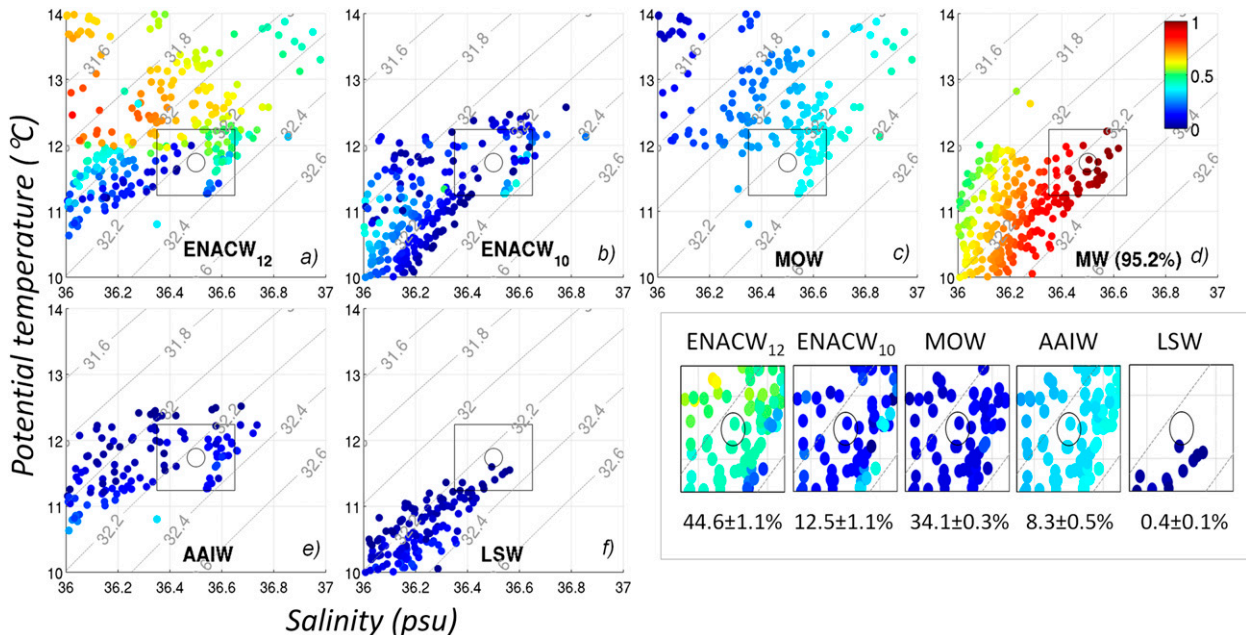
FIG. 4. Zoom of the potential temperature θ (surface reference level) vs salinity diagrams near the SWT for MW (open circle). (a)–(f) Each plot refers to a SWT, and colored scales represent the contribution of the SWTs (range between 0% and 100% for all SWTs). The black square delimits the area in which the percentage of the SWT contribution was averaged (mean contribution in parentheses). Gray dashed lines correspond to potential density anomaly at 1000-dbar reference level ($\sigma_1 = 31.6$ to 32.6 kg m^{-3}). The MW composition panel in the lower right shows the final decomposition of MW into its sources considering all data.

mean contribution of the SWTs within MF3 (with $i =$ ENACW$_{12}$, ENACW$_{10}$, AAIW, and MOW). Then, for the overall estimate within the defined θ–S interval, we considered both the MW–SWT decomposed contributions (Fig. 4d) and all the non-MW SWTs contributions (Figs. 4a–c,e,f). The final MW composition (Fig. 4, inlet gray rectangle) was obtained as the average ($\pm$standard deviation) of all SWT percentages in that thermohaline square.

The results obtained in this second step of the methodology will be shown and discussed in section 3.

3. Results and discussion

a. Water masses' contributions

1) SPATIAL DISTRIBUTION OF WATER MASSES

The distributions of the water masses' contributions X_i are shown in Figs. 5 and 6. In Fig. 5, we have defined five different vertical sections that tend to follow the path of the MOW flow off the Mediterranean Sea (sections A and B), its mixing and deepening in the GoC leading to the formation of MW (section C), and the export of the formed MW (once stabilized at intermediate depths; sections D and E). From east to west (from sections A to E, Fig. 5), the profile depth increases, as does the number of water masses

characterizing each section. In Fig. 6, the maximum contribution of each SWT in the latitude–longitude 2D plane is shown.

The upper 400 m of all sections are occupied by ENACW$_{18}$ and ENACW$_{12}$, which likely reach the GoC region as part of the Azores Current and/or recirculation of the Portugal Current. ENACW$_{18}$, whose maximum contribution is present at a mean pressure of 70 dbar, flows over ENACW$_{12}$, being most relevant in the central part of the GoC (Fig. 6). On the other hand, ENACW$_{12}$, with the maximum contribution at 360 dbar, affects a wider range in the water column (Fig. 6).

MOW presents its maximum contribution at 310 dbar within the Strait of Gibraltar (Fig. 6). Off the strait, it is a bottom-trapped density flow (Fig. 5, sections A and B). Note that MOW contribution isolines are parallel to σ_1 isopycnals (Fig. 5, gray dotted lines), with the densest core of MOW ($X_{MOW} > 50\%$) being well delimited by the $\sigma_1 = 32.4$ kg m^{-3} isopycnal [Fig. 5, sections A and B; where $\sigma_n =$ value for a potential density of (1000 + value) kg m^{-3} referred to as $n \times 1000$ db]. As it spreads, the MOW veers northward due to the Coriolis effect and progresses along the Iberian continental slope following the bathymetry until at least 7°W (Fig. 5, section C). There is a progressive deepening of MOW in the water column, accompanied by an intense mixing mostly with ENACW$_{12}$ (Fig. 5, sections A to C) that
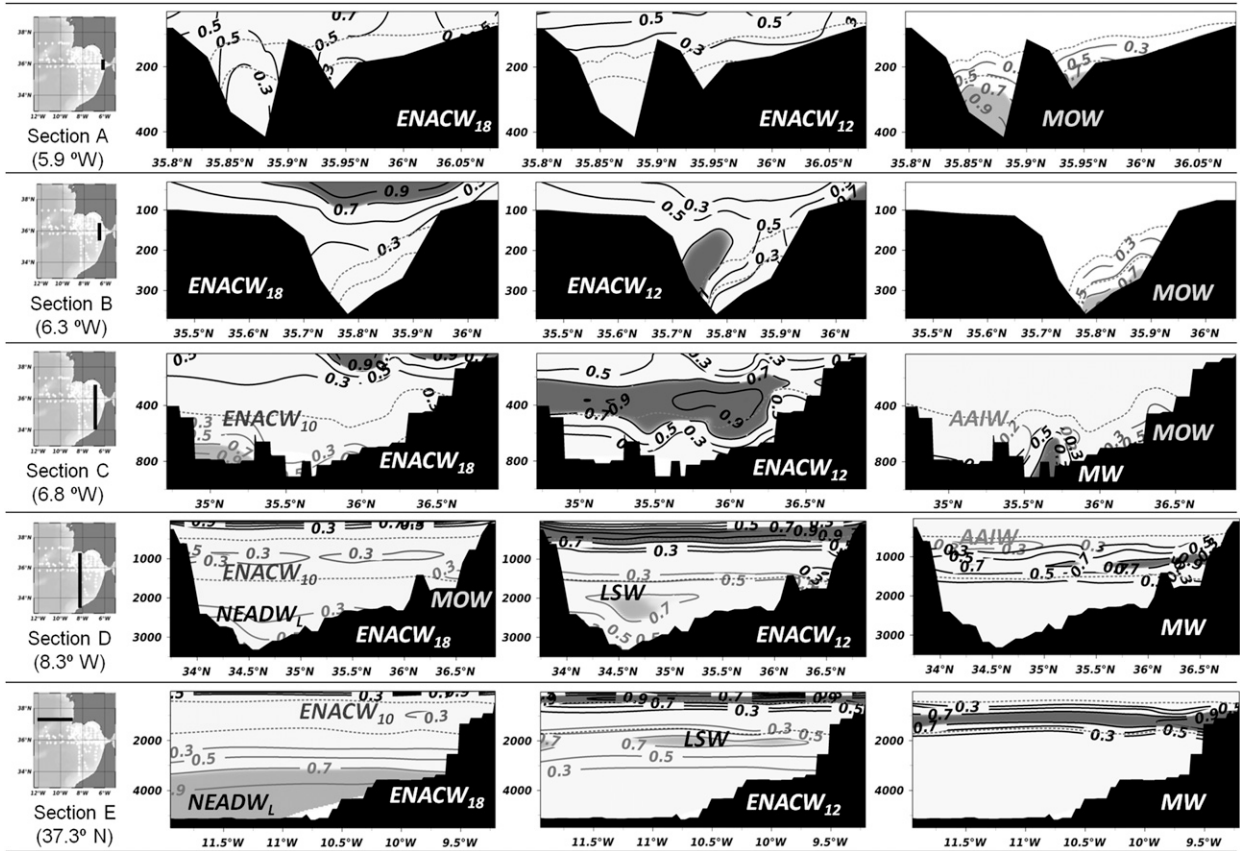
FIG. 5. SWTs' contributions along five different sections in the Gulf of Cádiz region. From east to west: meridional section A in the Strait of Gibraltar (5.9°W); meridional section B, west off Strait of Gibraltar (6.3°W); meridional section C in eastern Gulf of Cádiz (6.8°W); meridional section D (8.3°W) as defined by Louarn and Morin (2011); and zonal section E, near Cape St. Vincent (37.3°N). Dotted gray isolines are the potential density levels $\sigma_1 = 31.6$ and $32.4 \, \text{kg m}^{-3}$. Shaded areas highlight the water masses' percentages $> 70\%$.

diluts the MOW core. $ENACW_{10}$ reaches deeper layers (from 400 m to the bottom) of the southern part of section C (Fig. 5) because of the Ekman veering on its displacement eastward. The $ENACW_{10}$ core locates around 720 dbar and is present in the central area of the GoC (Fig. 6) and at the eastern side of section E (Fig. 5), close to the Iberian shelf.

In section C (Fig. 5), the features of the distribution of $ENACW_{10}$ together with those of MOW and MW indicate the recent formation of MW between 6.3° and 6.8°W. This result corroborates those of Rhein and Hinrichsen (1993), Johnson et al. (1994), and Baringer and Price (1997), among others, who delimited the area between 6.5°–7°W as the one where the process of formation of MW occurred. At 8.3°W (section D, Fig. 5), MW is stabilized at 1220 dbar (Fig. 6) and covers the 1000–1500-m depth range, below $ENACW_{10}$ (Fig. 5, sections D and E). The northward veering of the MW main vein can be deduced from the maximum contributions west of Cape St. Vincent in Fig. 6.

The presence of AAIW in the GoC, although relatively weak, can be corroborated. Mostly, it reaches this region with a maximum contribution of 35% (Fig. 6), but on average, it accounts for up to 17% of the characteristics of the waters in the GoC (Fig. 5, sections D and E; Fig. 6). Since we consider the SWT for AAIW as the one crossing the Lanzarote Passage, these results indicate that AAIW has experienced a 65% dilution until it reaches the GoC, where the degree of dilution will be more than 80% on average.

As for the deep waters, they are limited by depth (from about 1500 m to bottom), and they only participate in the characteristic of the outside regions of the domain (sections D and E, Fig. 6). Since LSW is situated over $NEADW_L$, it affects the inner regions of the GoC more than the latter. In fact, some mixing with the MW above can be deduced from section D distributions (Fig. 5). In section E (Fig. 5), both deep SWTs are clearly differentiated, with LSW characterizing mainly the ~2000-dbar east–west layer of the water column
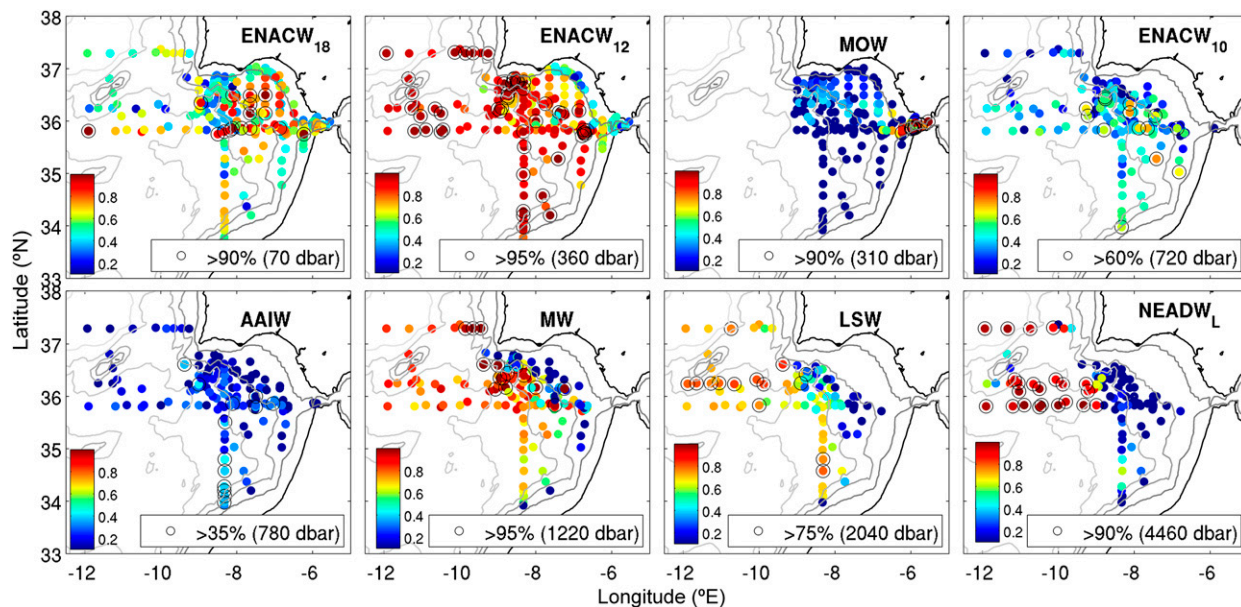
FIG. 6. Maximum SWTs contribution per station. Black open circles represent the highest contribution for each SWT. Pressures in parentheses represent the mean pressure of the respective SWT core (open circles).

and NEADW$_L$ limited to the western bottom layers of the section.

2) ANALYSIS OF THE WATER MASSES' CONTRIBUTIONS BY DENSITY LEVELS

Several studies in the GoC have dealt with the dynamic characterization of the westward density current related to the Mediterranean flow, broadly known as Mediterranean Undercurrent (Ambar and Howe 1979a; Ochoa and Bray 1991), differentiating between two velocity cores: an upper one at $\sigma_1 = 31.8\,\mathrm{kg\,m^{-3}}$, and a lower one at $\sigma_1 = 32.2\,\mathrm{kg\,m^{-3}}$. They directly related these cores to the thermohaline MW (upper and lower core) properties (Ambar and Howe 1979a,b; Ambar et al. 2002). More recently, Barbosa-Aguiar et al. (2015) also described these two eastward velocity cores: the lower one centered as in previous studies (at $\sigma_1 = 32.2\,\mathrm{kg\,m^{-3}}$) and the upper one located at the $\sigma_1 = 31.6$–$31.8\,\mathrm{kg\,m^{-3}}$ interval. However, in thermohaline terms, they identified just a single well-defined vein of saltier and warmer water, located at the 32.2–32.4 density range. This latter core is consistent with the MW end member defined from our OMP analysis.

To put our results into context, we selected those data points under the influence of the Mediterranean influence, that is, those within the thermohaline range of $8.64° \leq \theta \leq 14.14°\mathrm{C}$ and $35.7 \leq S \leq 38.4$ psu (Fig. 2, dashed square). The thermohaline extremes were chosen according to Barbosa-Aguiar et al. (2015) but with the upper salinity bound extended to MOW SWT

definition, in order to account for all MOW-influenced data points. The data within that interval were then divided into five density intervals between $31.6 \leq \sigma_1 \leq 32.6\,\mathrm{kg\,m^{-3}}$ (Barbosa-Aguiar et al. 2015) and in five zonal regions (defined so that they composed the sections shown in Fig. 5). For each layer and region, the water masses contributions obtained from eOMP were averaged. Despite the fact that the number of samples per layer and level (see Table 5) can be a limiting factor, we will highlight some interesting remarks in view of our results.

Close to the Strait of Gibraltar (regions 1 and 2, between 5.5° and 6.5°W), the water masses' mixing consists just of ENACW$_{18}$, ENACW$_{12}$, and MOW. The mixing is quite homogeneous both vertically and horizontally but shows a logical vertical increasing (decreasing) gradient in the MOW (ENACW$_{12}$) contribution. In the lightest layer, there is a lateral change in the ENACW$_{18}$/ENACW$_{12}$ proportion, with ENACW$_{18}$ reducing its presence more than half in region 2 with respect to region 1 at the expense of ENACW$_{12}$. This change could be a reflection of the differential mixing between MOW and central waters of different temperatures (Ambar and Howe 1979a). However, we have to take into account that, in region 1, the density range $31.6 \leq \sigma_1 \leq 32.6\,\mathrm{kg\,m^{-3}}$ comprises the interface between the central waters inflow and the MOW outflow (Barbosa-Aguiar et al. 2015), which is an active thick transitional interface layer in which the speed of the water flow changes gradually in the vertical

(Sannino et al. 2009), resulting in a net horizontal transport (Bray et al. 1995). However, lacking the dynamics of the layer, we cannot assure that the lateral change in the $ENACW_{18}$ presence means that is being incorporated to the outflow.

As shown in the previous section, MW starts to appear as a water mass body with its own thermohaline and chemical characteristics from region 3 (6.5°W) onward, coinciding with the appearance of AAIW and $ENACW_{10}$, which will contribute to MW formation. We can differentiate two main steps of formation: first, appearing in the lightest density range 31.6 to 32.4 kg m^{-3} at region 3, and, second, appearing in the densest 32.4–32.6 kg m^{-3} level between regions 3 and 4. There is evidence that this second mixing process will lead to a diapycnal MW flow, from 32.4 to 32.6 kg m^{-3} (region 4) to the 32.2 to 32.4 kg m^{-3} density level (region 5); that is, not only the diapycnal fluxes will occur as result of the cascading of MOW to deeper levels while becoming MW, but MW, once already formed at region 4, also suffers diapycnal readjustment until it reaches its "natural" buoyancy at 32.2–32.4 kg m^{-3}, in the vicinity of Cape St. Vincent.

b. Mediterranean Water composition and export off the Gulf of Cádiz

From the procedure described in section 2 [section 2b(2)(ii)], we determined that MW is composed by 57.1% of central waters (44.6% $\pm$ 1% of $ENACW_{12}$ and 12.5% $\pm$ 1% of $ENACW_{10}$), 34.1% $\pm$ 0.3% of MOW, 8.3% $\pm$ 0.5% of AAIW, and a small contribution of 0.4% $\pm$ 0.1% of LSW. This result is compatible (within the standard deviation) with the first guess (the step one of the methodology): 50% $\pm$ 9% of $ENACW_{12}$, 5% $\pm$ 11% of $ENACW_{10}$, 34% $\pm$ 3% of MOW, 7% $\pm$ 8% of AAIW, and 4% $\pm$ 6% of LSW. Both results do not show significant differences, but the MW composition is more accurate by using the second step, which presents lower STDs in the contributions than the first guess. Besides, considering the results from the first guess, the contribution of LSW can be as important as that of AAIW, and that would not be an appropriate consideration for defining MW. The first step, however, is really helpful and reliable enough to obtain a first guess of the properties of MW in order to be included as a SWT in the second step of the methodology.

Considering the obtained decomposition and the properties of the SWT sources of MW, the thermohaline properties of MW were reconstructed following Eq. (1). This in situ redefinition of the MW SWT provides θ and S values consistent with the bibliography (11.81° $\pm$ 0.2°C, 36.53 $\pm$ 0.07 psu; Table 4). For oxygen and nutrients, we obtained a new redefinition for the MW SWT

of $O_2^0 = 213 \pm 7$, $SiO_2^0 = 7.0 \pm 0.6$, $NO_3^0 = 9.9 \pm 1.1$, and $PO_4^0 = 0.56 \pm 0.07 \,\mu$mol kg^{-1}. Previous references (Table 4) agree in degree more or less with our results.

The ENACW:MOW mixing ratio obtained here (57.1%:34.1%) is compatible with those given by Zenk (1975; 68%:32%) or Rhein and Hinrichsen (1993; 66%:34%). The differences are due to the contribution of AAIW and LSW here considered, which were not included in either of the before cited studies. The participation of AAIW in the formation of MW was first quantified by Louarn and Morin (2011). The difference between our results and theirs are mostly due to the different SWTs considered. Their AAIW and LSW SWTs' definitions correspond to more diluted varieties, which, in terms of the OMP, will lead to higher proportions of both water masses in the mixing to form MW.

Having taken into account that the mean annual MOW transport at the Strait of Gibraltar (Camarinal Sill) is of 0.74 $\pm$ 0.05 Sv, according to the most recent estimations of García-Lafuente et al. (2011), and under a first reasonable assumption that all MOW becomes MW, we approximated the MW formation rate, that is, the total volume of MW likely to leave the GoC, as 2.17 Sv (i.e., 0.74 Sv of MOW, 0.97 Sv of $ENACW_{12}$, 0.27 Sv of $ENACW_{10}$, 0.18 Sv of AAIW, and 0.01 Sv of LSW). This result is comparable to the traditionally reported values of 2–3 (Zenk 1975), 2.6 (Ambar and Howe 1979b), 2.2 (Ochoa and Bray 1991), 2.9 (Rhein and Hinrichsen 1993), 1.9 (Baringer and Price 1997), or 2.3 Sv (Álvarez et al. 2005). From this total volume, 1.25 Sv would correspond to the entrainment of ENACW, in good agreement with the estimate by Baringer and Price (1997) of 1.3 Sv, by Alves et al. (2011) of 1.2–1.7 Sv (with a mean value of 1.4 Sv), or 1.1 Sv by Barbosa-Aguiar et al. (2015).

However, Barbosa-Aguiar et al. (2015) demonstrated, by means of a Lagrangian analysis, that when MOW reaches 8.5°W (their section II), a vast majority (70%) ends up in the layer $\sigma_1 = 32.2$–32.4 kg m^{-3}, while 11.6% and 11.2% spread to the immediately upper ($\sigma_1 = 32.0$–32.2 kg m^{-3}) and lower ($\sigma_1 = 32.4$–32.6 kg m^{-3}) adjacent layers, respectively. Just the remaining MOW small proportion (<8%) would go in the upper MW core. As we considered the MW spreading in the North Atlantic to be the water mass with an SWT that is defined by the θ–S properties 11.74° $\pm$ 0.5°C and 36.5 $\pm$ 0.15 psu, centered in the 32.2–32.4 kg m^{-3} density range; we can redo the volume estimates taking into account that not all MOW flowing out the Strait of Gibraltar will take part of this MW core but 70%. Under this second consideration, the

TABLE 5. Mean SWTs contributions (%) in the main density range in which Mediterranean waters have influence ($31.6 \leq \sigma_1 \leq 32.6 \, \mathrm{kg \, m^{-3}}$, with a thermohaline range of $8.64° \leq \theta \leq 14.14°C$ and $35.7 \leq S \leq 38.4$), averaged by five density layers ($0.2 \, \mathrm{kg \, m^{-3}}$ intervals) and delimited by longitude in five geographic regions (5.5°–6°W, 6°–6.5°W, 6.5°–7°W, 7°–9.3°W, and 9.3°–12°W).

	Region 5 (9.3°–12°W)							Region 4 (7°–9.3°W)								
	$ENACW_{12}$	$ENACW_{10}$	AAIW	MW	LSW	$NEADW_L$	No. data	$ENACW_{18}$	$ENACW_{12}$	MOW	$ENACW_{10}$	AAIW	MW	LSW	$NEADW_L$	No. data
Layer 1 (31.6–31.8)	57	14	3	27			(9)	2	63	5	8	9	13			(30)
Layer 2 (31.8–32.0)	30	17	10	42			(26)	2	42	8	11	10	26			(142)
Layer 3 (32.0–32.2)	4	21	2	68	2	3	(39)		15	6	23	2	47	2	3	(198)
Layer 4 (32.2–32.4)		6		80	12	2	(31)		11	10	8	2	57	9	2	(169)
Layer 5 (32.4–32.6)													67	28	5	(4)

final volume of MW we could expect from our MW contributions' decomposition would be 1.52 Sv (i.e., 0.52 Sv of MOW, 0.68 Sv of $ENACW_{12}$, 0.19 Sv of $ENACW_{10}$, 0.13 Sv of AAIW, and <0.01 Sv of LSW). This value agrees with the Carracedo et al. (2015) estimate for MW exportation (SWT for MW defined like in the present study, 11.74°C and 36.5 psu) from climatologic data (1.61 ± 0.15 Sv) and CAIBOX-2009 quasi-synoptic summer data (1.5 ± 0.4 Sv).

The difference between both MW volume estimates (1.5 or 2.2 Sv) remains in the definition of MW itself, that is, if we just focus on the spreading of the thermohaline extreme properties (here understood as MW core, $\sigma_1 = 32.2$–$32.4 \, \mathrm{kg \, m^{-3}}$) or, on the contrary, we account for the whole Mediterranean Undercurrent (broader density range $\sigma_1 = 31.6$–$32.6 \, \mathrm{kg \, m^{-3}}$). Added to the fact that the velocity veins and the thermohaline anomaly cores are not collocated (Barbosa-Aguiar et al. 2015), all of this makes the interpretation and comparison of results from both points of view need to be considered with caution. That is, when comparing MW exportation rates, it is crucial to pay attention to the thermohaline and chemical definition of MW as well as to the density ranges of the flow estimate.

4. Summary and conclusions

In the present work, we have quantified the mixing of the water masses in the GoC region using a least squares regression, OMP analysis. Based on θ, S, SiO_2, NO_3, PO_4, and O_2, the OMP analysis was applied on a broad compilation of data spanning between 33.5° and 38°N and 5.5° and 12°W. The sensitivity of the analysis to sources of error in the measured parameters and the SWTs properties were evaluated using a perturbation test.

This methodology allowed us to describe the core water masses' distributions. Subtropical Central Waters enter along the Strait of Gibraltar toward the Mediterranean Sea, while MOW flows westward constrained to the northward continental shelf of the Gulf of Cadiz. Subpolar Central Water occupies the center and southern regions of the domain, being mainly entrained into the MOW between 6.3° and 6.8°W. Mixed with Subpolar Central Water, AAIW effectively reaches the region having experienced around 80% of dilution since it crosses the Lanzarote Passage between the Canary Islands and the African coast.

This study quantifies the composition of the MW thermohaline extreme, once stabilized at about 1200 dbar south of Cape St. Vincent (8°–9°W), thus providing a general definition of this water mass formed in the GoC. This water mass core corresponds to the widely used θ–S extreme point characterizing MW in the eastern North Atlantic, whose mean properties were reestimated in this study as $\theta = 11.81° \pm 0.2°C$, $S = 36.53 \pm 0.07$ psu, $O_2^0 = 213 \pm 7$, $SiO_2^0 = 7.0 \pm 0.6$, $NO_3^0 = 9.9 \pm 1.1$, and $PO_4^0 = 0.56 \pm 0.07 \, \mu mol \, kg^{-1}$. We determined MW to be composed by 57.1% of central waters (44.6% ± 1% of $ENACW_{12}$ and 12.5% ± 1% of $ENACW_{10}$), 34.1% ± 0.3% of MOW, 8.3% ± 0.5% of AAIW, and the small contribution of 0.4% ± 0.1% of LSW. There is evidence of a differential mixing between MOW and central waters, pointing out to two main steps of formation: first in the lightest density range 31.6 to $32.4 \, \mathrm{kg \, m^{-3}}$ between 6.5° and 7°W and second in the densest 32.4–$32.6 \, \mathrm{kg \, m^{-3}}$ level between 7° and 9°W, where deepest MW transformation takes place. Once MW is formed, there is sign of diapycnal readjustment until it reaches its natural buoyancy at 32.2–$32.4 \, \mathrm{kg \, m^{-3}}$, close to Cape St. Vincent. Finally, by assuming all MOW is involved in MW formation, we inferred a formation rate for MW of 2.2 Sv, comprising

TABLE 5. (*Extended*)

Region 3 (6.5°–7°W)								Region 2 (6°–6.5°W)				Region 1 (5.5°–6°W)			
ENACW$_{18}$	ENACW$_{12}$	MOW	ENACW$_{10}$	AAIW	MW	NEADWL	No. data	ENACW$_{18}$	ENACW$_{12}$	MOW	No. data	ENACW$_{18}$	ENACW$_{12}$	MOW	No. data
10	64	11	4	3	8		(8)	10	75	15	(3)	26	57	17	(3)
4	40	11	16	6	23		(13)	21	52	26	(3)	14	61	25	(1)
2	38	19	6	4	31		(7)	15	44	41	(2)	20	42	38	(4)
4	34	29			28	5	(3)	15	36	49	(3)	19	35	46	(1)
1	39	49	12				(2)	17	23	60	(2)	15	26	59	(6)

0.97 Sv of ENACW$_{12}$, 0.27 Sv of ENACW$_{10}$, 0.74 Sv of MOW, 0.18 Sv of AAIW, and 0.01 Sv of LSW. This means a central waters entrainment of 1.26 Sv.

When comparing MW exportation rates, the need for paying special attention to the definition followed to account for the Mediterranean Water mass and to the density ranges in which we are basing our definition has been highlighted. Whether we are referring to the thermohaline extreme that can be traced by OMP analysis in the wide North Atlantic, as we aimed in this study, or whether we are studying the dynamics of the westward Mediterranean-influenced undercurrent, both approaches are valid but could comprise different water mass volumes.

APPENDIX A

Specifications of the OMP Analysis

In this work, we applied a methodology previously used and validated in different studies (Pardo et al. 2012; Carracedo et al. 2012; García-Ibáñez et al. 2015), in which a more detailed description can be found.

Briefly, we perform an extended OMP (eOMP) analysis (Karstensen and Tomczak 1998) using θ, S, and SiO$_2$ as conservative variables and NO$_3$, PO$_4$, and O$_2$ as nonconservative variables; these latter variables were affected by the process of remineralization of the organic matter. This process is represented in the eOMP analysis by a new unknown (ΔO; Tables 4, A1), which is the oxygen consumed in the sample due to the respiration of organic matter and relates to the corresponding variables through predefined stoichiometric coefficients. The stoichiometric coefficients considered for O$_2$ consumption (from the initial close-to-saturation conditions) into NO$_3$ and PO$_4$ were $r_N = 9.3$ and $r_P = 149$ (Fraga et al. 1998; Pérez et al. 2001; Álvarez et al. 2005). The final result from the eOMP analysis is the contribution to the mixing of each SWT i (X_i) in each water sample for the corresponding MF (section

TABLE A1. System of equations of the eOMP analysis. The W are the weights of each equation; θ_{obs}, S_{obs}, SiO$_{2obs}$, O$_{2obs}$, NO$_{3obs}$, and PO$_{4obs}$ are the sampled properties; θ_i, S_i, SiO$_{2i}^0$, O$_{2i}$, NO$_{3i}^0$, and PO$_{4i}^0$ are the properties of the ith SWT (the superscript 0 refers to preformed values); and R is the residual of each variable (referred to by the subscript) that the eOMP seeks to minimize.

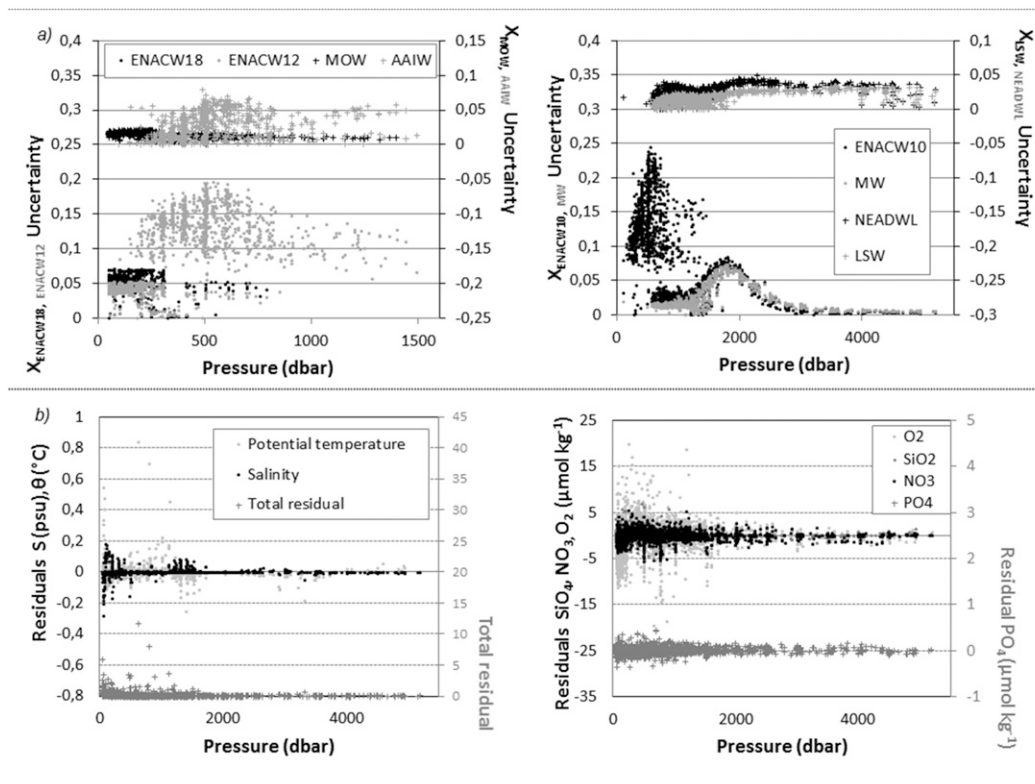| eOMP	W
$1 = \sum_{i=1}^{nSWT} X_i + R_x$ (A1)	100
$\theta_{obs} = \sum_{i=1}^{nSWT} X_i \theta_i + R_{\theta_{obs}}$ (A2)	20
$S_{obs} = \sum_{i=1}^{nSWT} X_i S_i + R_{S_{obs}}$ (A3)	10
$SiO_{2obs} = \sum_{i=1}^{nSWT} X_i SiO_{2i}^0 + R_{SiO_{2obs}}$ (A4)	4
$NO_{3obs} = \sum_{i=1}^{nSWT} X_i NO_{3i}^0 + \dfrac{\Delta O}{r_N} + R_{NO_{3obs}}$ (A5)	1
$PO_{4obs} = \sum_{i=1}^{nSWT} X_i PO_{4i}^0 + \dfrac{\Delta O}{r_P} + R_{PO_{4obs}}$ (A6)	1
$O_{2obs} = \sum_{i=1}^{nSWT} X_i O_{2i} - \Delta O + R_{O_{2obs}}$ (A7)	1

FIG. B1. (a) Uncertainties of the contributions (standard deviation resulting from 100 perturbed contribution fields) by depth. Dots refer to left axis and crosses to the right axis. (b) Residuals (modeled value minus observed value) for the six variables used in the eOMP [(left) θ, S, and total residual and (right) SiO_2, NO_3, PO_4, and O_2].

2b), which has been selected previously to apply the eOMP. MF selection procedure is detailed in Pardo et al. (2012) and García-Ibáñez et al. (2015).

The system of equations is shown in Table A1. The equations are normalized, using the mean and standard deviation of the properties of each SWT (Table 3) and weighted W in the function of the accuracy of the measured property (Tomczak 1981). The weights were adjusted so that the ratios between the standard error of the estimate (SDR; Table 3) and the analytical error ε (Table 3) were almost the same for all the SWTs properties (SDR/ε; Table 3; Álvarez et al. 2005). As a constraint to the minimization process, mass conservation must be rigorously satisfied [Table A1; Eq. (A1)]; hence, it takes the highest weight. Besides, the contribution of each SWT must be positive.

To reduce the error of the whole OMP analysis, the resolution algorithm of this methodology involves an iterative procedure for nutrients (Álvarez et al. 2004) that comprises all the samples, since they accumulate the highest errors. Within this iterative process, SiO_2, NO_3, and PO_4 of the SWTs are reconstructed each time [Table A1; Eqs. (A4), (A5), and (A6)]. These new estimates (note differences between initial and final values are small; Table 3) are assigned to the SWTs and the methodology is rerun until

the total residual reaches an asymptote. This procedure successively reduces the residuals on those variables and hence the error of the whole OMP analysis (Álvarez et al. 2004, 2005; Pardo et al. 2012). Five iterations are enough to reach that premise. Note, however, that the mean percentage of change in the SWT nutrients is low (3%, 5%, and 6% for SiO_2, NO_3, and PO_4, respectively).

The model ability to reproduce the measured values is given as the correlation coefficient r^2 (Table 3) between the measured and modeled values. The fact that the r^2 is higher than 0.97 for any of the variables highlights the reliability of the OMP analysis. More about the robustness (assured on the basis of a perturbation analysis; Lawson and Hanson 1974) and accuracy (residuals of the system) is detailed in appendix B.

APPENDIX B

Robustness of the OMP Analysis: Perturbations and Residuals

The robustness of the OMP analysis has been broadly assessed in detail in previous studies (Álvarez

et al. 2004, 2005, 2014; Pardo et al. 2012; García-Ibáñez et al. 2015). Thinking about the reliability of this kind of method, one of the main considerations is the non-stationary nature of the SWTs properties, which acts as a source of uncertainty. We certainly know that the properties of the SWTs may fluctuate or change over time at their geographical origin (source regions). To account, in a certain manner, for such variability, we have performed a perturbation analysis of uncertainties. On one hand, we have randomly modified the SWTs properties and, on the other hand (to account for uncertainties in the measured variables), the field data, both following a normal distribution, with (i) the property as the mean value and (ii) the accuracy of the variable as its standard deviation. The standard deviations of the SWTs are shown in Table 4. In the case of the standard deviations for the field data, we used 0.005°C, 0.01 psu, and 0.5, 0.2, 0.02, and $3\,\mu\text{mol kg}^{-1}$ for θ, S, SiO_2, NO_3, PO_4, and O_2, respectively. A total of 100 perturbations were performed (Álvarez et al. 2004, 2005; Pardo et al. 2012), that is, we obtained 100 different solutions (100 X_i arrays for each SWT i) from which we have estimated the mean and the standard deviation (Fig. B1a). As previously mentioned, apart from giving an idea of the stability of the system, this standard deviation (for each single point) was used as the uncertainty of the method. In general, the mean SWTs' distributions slightly differ from the solution without perturbations, and the standard deviations of such contributions rarely exceed 10%.

Once the water mass mixing is solved, the property fields can be reconstructed with the values of the contributions (X_i) and of the properties of the SWTs. The difference between the values obtained and the observed ones is what are known as residuals. These residuals account for the nonconservative component of the nutrients and for possible errors in the measurements. A reference value of the reliability of the method is provided by the sum of the squares of the set of those residuals, known as the total residual (or total error of the method; Pardo et al. 2012). In Fig. B1b (left panel), we present the total residual by pressure levels. Higher values are located in the upper levels of the water column because of the variability induced by air–sea interaction. The mean value of the total residual is 0.46, which is notably reduced to a closer-to-zero value (0.081) by disregarding the first 400 dbar of the water column.

If we pay attention to the residuals by variables (Fig. B1b), θ and S are better fitted than the others, as they have the highest weights in the analysis, with 0.046 and 0.009 as the respective standard deviations of their residuals (below 400 dbar; see SDR in Table 3). The O_2

residuals mainly range between $\pm 5\,\mu\text{mol kg}^{-1}$, those of SiO_2 and NO_3 range between $\pm 1\,\mu\text{mol kg}^{-1}$, and those of PO_4 range between $\pm 0.1\,\mu\text{mol kg}^{-1}$, with 3.2, 1.1, 0.69, and 0.069 as the respective standard deviations of the residuals (deeper than 400 dbar). These values mostly respond to the weight assigned to each property in the OMP analysis.

REFERENCES

Àlvarez, M., F. F. Pérez, H. Bryden, and A. F. Ríos, 2004: Physical and biogeochemical transports structure in the North Atlantic Subpolar Gyre. *J. Geophys. Res.*, **109**, C03027, doi:10.1029/2003JC002015.

——, ——, D. R. Shoosmith, and H. L. Bryden, 2005: Unaccounted role of Mediterranean Water in the drawdown of anthropogenic carbon. *J. Geophys. Res.*, **110**, C09S03, doi:10.1029/2004JC002633.

——, S. Brea, H. Mercier, and X. A. Álvarez-Salgado, 2014: Mineralization of biogenic materials in the water masses of the South Atlantic Ocean. I: Assessment and results of an optimum multiparameter analysis. *Prog. Oceanogr.*, **123**, 1–23, doi:10.1016/j.pocean.2013.12.007.

Álvarez-Salgado, X. A., M. Álvarez, S. Brea, L. Mèmery, and M. J. Messias, 2014: Mineralization of biogenic materials in the water masses of the South Atlantic Ocean. II: Stoichiometric ratios and mineralization rates. *Prog. Oceanogr.*, **123**, 24–37, doi:10.1016/j.pocean.2013.12.009.

Alves, J. M. R., X. Carton, and I. Ambar, 2011: Hydrological structure, circulation and water mass transport in the Gulf of Cadiz. *Int. J. Geosci.*, **2**, 432–456, doi:10.4236/ijg.2011.24047.

Ambar, I., 1983: A shallow core of Mediterranean Water off western Portugal. *Deep-Sea Res.*, **30A**, 677–680, doi:10.1016/0198-0149(83)90045-6.

——, and M. R. Howe, 1979a: Observations of the Mediterranean outflow—I Mixing in the Mediterranean outflow. *Deep-Sea Res.*, **26**, 535–554, doi:10.1016/0198-0149(79)90095-5.

——, and ——, 1979b: Observations of the Mediterranean outflow—II The deep circulation in the vicinity of the Gulf of Cadiz. *Deep-Sea Res.*, **26A**, 555–568, doi:10.1016/0198-0149(79)90096-7.

——, L. Armi, A. Bower, and T. Ferreira, 1999: Some aspects of time variability of the Mediterranean Water off south Portugal. *Deep-Sea Res. I*, **46**, 1109–1136, doi:10.1016/S0967-0637(99)00006-0.

——, N. Serra, M. J. Brogueira, G. Cabeçadas, F. Abrantes, P. Freitas, C. Gonçalves, and N. Gonzalez, 2002: Physical, chemical and sedimentological aspects of the Mediterranean outflow off Iberia. *Deep-Sea Res. II*, **49**, 4163–4177, doi:10.1016/S0967-0645(02)00148-0.

Arhan, M., 1987: On the large scale dynamics of the Mediterranean outflow. *Deep-Sea Res.*, **34A**, 1187–1208, doi:10.1016/0198-0149(87)90071-9.

——, and B. King, 1995: Lateral mixing of the Mediterranean Water in the eastern North Atlantic. *J. Mar. Res.*, **53**, 865–895, doi:10.1357/0022240953212990.

Barbosa-Aguiar, A. C., A. Peliz, F. Neves, I. Bashmachnikov, and X. Carton, 2015: Mediterranean outflow transports and entrainment estimates from observations and high-resolution modelling. *Prog. Oceanogr.*, **131**, 33–45, doi:10.1016/j.pocean.2014.11.008.

Baringer, M. O., and J. F. Price, 1997: Mixing and spreading of the Mediterranean outflow. *J. Phys. Oceanogr.*, **27**, 1654–1677, doi:10.1175/1520-0485(1997)027<1654:MASOTM>2.0.CO;2.

——, and ——, 1999: A review of the physical oceanography of the Mediterranean outflow. *Mar. Geol.*, **155**, 63–82, doi:10.1016/S0025-3227(98)00141-8.

Bower, A. S., L. Armi, and I. Ambar, 1995: Direct evidence of meddy formation off the southwestern coast of Portugal. *Deep-Sea Res. I*, **42**, 1621–1630, doi:10.1016/0967-0637(95)00045-8.

Brambilla, E., and L. D. Talley, 2008: Subpolar Mode Water in the northeastern Atlantic: 1. Averaged properties and mean circulation. *J. Geophys. Res.*, **113**, C04025, doi:10.1029/2006JC004062.

Bray, N. A., J. Ochoa, and T. H. Kinder, 1995: The role of the interface in exchange through the Strait of Gibraltar. *J. Geophys. Res.*, **100**, 10 755–10 776, doi:10.1029/95JC00381.

Carracedo, L. I., P. C. Pardo, N. Villacieros-Robineau, F. De la Granda, M. Gilcoto, and F. F. Pérez, 2012: Temporal changes in the water mass distribution and transports along the 20°W CAIBOX section (NE Atlantic). *Cienc. Mar.*, **38**, 263–286, doi:10.7773/cm.v38i1B.1793.

——, M. Gilcoto, H. Mercier, and F. F. Pérez, 2014: Seasonal dynamics in the Azores–Gibraltar Strait region: A climatologically-based study. *Prog. Oceanogr.*, **122**, 116–130, doi:10.1016/j.pocean.2013.12.005.

——, ——, ——, and ——, 2015: Quasi-synoptic transport, budgets and water mass transformation in the Azores–Gibraltar Strait region during summer 2009. *Prog. Oceanogr.*, **130**, 47–64, doi:10.1016/j.pocean.2014.09.006.

Castro, C. G., F. F. Pérez, S. E. Holley, and A. F. Rìos, 1998: Chemical characterisation and modelling of water masses in the northeast Atlantic. *Prog. Oceanogr.*, **41**, 249–279, doi:10.1016/S0079-6611(98)00021-4.

Criado-Aldeanueva, F., J. García-Lafuente, J. M. Vargas, J. Del Río, A. Vázquez, A. Reul, and A. Sánchez, 2006: Distribution and circulation of water masses in the Gulf of Cadiz from in situ observations. *Deep-Sea Res. II*, **53**, 1144–1160, doi:10.1016/j.dsr2.2006.04.012.

Dickson, R. R., and J. Brown, 1994: The production of North Atlantic Deep Water: Sources, rates, and pathways. *J. Geophys. Res.*, **99**, 12 319–12 341, doi:10.1029/94JC00530.

Emery, W. J., and J. Meincke, 1986: Global water masses: Summary and review. *Oceanol. Acta*, **9**, 383–391.

Fiúza, A. F. G., M. Hamann, I. Ambar, G. Dìaz del Rìo, N. González, and J. M. Cabanas, 1998: Water masses and their circulation off western Iberia during May 1993. *Deep-Sea Res. I*, **45**, 1127–1160, doi:10.1016/S0967-0637(98)00008-9.

Flecha, S., F. F. Pérez, G. Navarro, J. Ruiz, I. Olivé, S. Rodríguez-Gálvez, E. Costas, and I. E. Huertas, 2012: Anthropogenic carbon inventory in the Gulf of Cádiz. *J. Mar. Syst.*, **92**, 67–75, doi:10.1016/j.jmarsys.2011.10.010.

Fraga, F., A. F. Ríos, F. F. Pérez, and F. G. Figueiras, 1998: Theoretical limits of oxygen:carbon and oxygen:nitrogen ratios during photosynthesis and mineralisation of organic matter in the sea. *Sci. Mar.*, **62**, 161–168, doi:10.3989/scimar.1998.62n1-2161.

Fusco, G., V. Artale, Y. Cotroneo, and G. Sannino, 2008: Thermohaline variability of Mediterranean Water in the Gulf of Cadiz, 1948–1999. *Deep-Sea Res. I*, **55**, 1624–1638, doi:10.1016/j.dsr.2008.07.009.

García-Ibáñez, M. I., P. C. Pardo, L. I. Carracedo, H. Mercier, P. Lherminier, A. F. Ríos, and F. F. Pérez, 2015: Structure, transports and transformations of the water masses in the Atlantic Subpolar Gyre. *Prog. Oceanogr.*, **135**, 18–36, doi:10.1016/j.pocean.2015.03.009.

García-Lafuente, J., A. Sánchez Román, G. Díaz del Río, G. Sannino, and J. C. Sánchez Garrido, 2007: Recent observations of seasonal variability of the Mediterranean outflow in the Strait of Gibraltar. *J. Geophys. Res.*, **112**, C10005, doi:10.1029/2006JC003992.

——, ——, C. Naranjo, and J. C. Sánchez-Garrido, 2011: The very first transformation of the Mediterranean outflow in the Strait of Gibraltar. *J. Geophys. Res.*, **116**, C07010, doi:10.1029/2011JC006967.

Gascard, J. C., and C. Richez, 1985: Water masses and circulation in the western Alboran Sea and in the Strait of Gibraltar. *Prog. Oceanogr.*, **15**, 157–216, doi:10.1016/0079-6611(85)90031-X.

Harvey, J., 1982: θ-S relationships and water masses in the eastern North Atlantic. *Deep-Sea Res.*, **29A**, 1021–1033, doi:10.1016/0198-0149(82)90025-5.

Howe, M. R., M. I. Abdullah, and S. Deetae, 1974: An interpretation of the double T-S maxima in the Mediterranean outflow using chemical tracers. *J. Mar. Res.*, **32**, 377–386.

Huertas, I. E., and Coauthors, 2012: Atlantic forcing of the Mediterranean oligotrophy. *Global Biogeochem. Cycles*, **26**, GB2022, doi:10.1029/2011GB004167.

Iorga, M. C., and M. S. Lozier, 1999a: Signatures of the Mediterranean outflow from a North Atlantic climatology: 1. Salinity and density fields. *J. Geophys. Res.*, **104**, 25 985–26 009, doi:10.1029/1999JC900115.

——, and ——, 1999b: Signatures of the Mediterranean outflow from a North Atlantic climatology: 2. Diagnostic velocity fields. *J. Geophys. Res.*, **104**, 26 011–26 029, doi:10.1029/1999JC900204.

Ito, T., M. J. Follows, and E. A. Boyle, 2004: Is AOU a good measure of respiration in the oceans? *Geophys. Res. Lett.*, **31**, L17305, doi:10.1029/2004GL020900.

Jia, Y., 2000: Formation of an Azores Current due to Mediterranean overflow in a modeling study of the North Atlantic. *J. Phys. Oceanogr.*, **30**, 2342–2358, doi:10.1175/1520-0485(2000)030<2342:FOAACD>2.0.CO;2.

Johnson, G. C., 2008: Quantifying Antarctic Bottom Water and North Atlantic Deep Water volumes. *J. Geophys. Res.*, **113**, C05027, doi:10.1029/2007JC004477.

——, T. B. Sanford, and M. O'Neil Baringer, 1994: Stress on the Mediterranean outflow plume: Part I. Velocity and water property measurements. *J. Phys. Oceanogr.*, **24**, 2072–2083, doi:10.1175/1520-0485(1994)024<2072:SOTMOP>2.0.CO;2.

Karstensen, J., and M. Tomczak, 1997: Ventilation processes and water mass ages in the thermocline of the southeast Indian Ocean. *Geophys. Res. Lett.*, **24**, 2777–2780, doi:10.1029/97GL02708.

——, and ——, 1998: Age determination of mixed water masses using CFC and oxygen data. *J. Geophys. Res.*, **103**, 18 599–18 609, doi:10.1029/98JC00889.

Keffer, T., 1985: The ventilation of the world's oceans: Maps of the potential vorticity field. *J. Phys. Oceanogr.*, **15**, 509–523, doi:10.1175/1520-0485(1985)015<0509:TVOTWO>2.0.CO;2.

Lawson, C. L., and R. J. Hanson, 1974: *Solving Least Squares Problems.* Prentice-Hall, 340 pp.

Lionello, P., P. Malanotte-Rizzoli, and R. Boscolo, 2006: *Mediterranean Climate Variability.* Elsevier, 439 pp.

Lønborg, C., and X. A. Álvarez-Salgado, 2014: Tracing dissolved organic matter cycling in the eastern boundary of the temperate North Atlantic using absorption and fluorescence

spectroscopy. *Deep-Sea Res. I*, **85**, 35–46, doi:10.1016/j.dsr.2013.11.002.

Louarn, E., and P. Morin, 2011: Antarctic Intermediate Water influence on Mediterranean Sea Water outflow. *Deep-Sea Res. I*, **58**, 932–942, doi:10.1016/j.dsr.2011.05.009.

Machín, F., and J. L. Pelegrí, 2009: Northward penetration of Antarctic Intermediate Water off northwest Africa. *J. Phys. Oceanogr.*, **39**, 512–535, doi:10.1175/2008JPO3825.1.

——, A. Hernández-Guerra, and J. L. Pelegrí, 2006: Mass fluxes in the Canary basin. *Prog. Oceanogr.*, **70**, 416–447, doi:10.1016/j.pocean.2006.03.019.

——, J. L. Pelegrí, E. Fraile-Nuez, P. Vélez-Belchí, F. López-Laatzen, and A. Hernández-Guerra, 2010: Seasonal flow reversals of intermediate waters in the Canary Current system east of the Canary Islands. *J. Phys. Oceanogr.*, **40**, 1902–1909, doi:10.1175/2010JPO4320.1.

Madelain, F., 1970: Influence de la topographie du fond sur l'ecoulement Mediterranean entre le detroit de Gibraltar et le Cap Saint-Vincent. *Cah. Oceanogr.*, **22**, 43–61.

Malakoff, D., 2014: Chemical atlas shows where seas are tainted—And where they can bloom. *Science*, **343**, 1070–1070, doi:10.1126/science.343.6175.1070.

McCartney, M. S., and L. D. Talley, 1982: The Subpolar Mode Water of the North Atlantic Ocean. *J. Phys. Oceanogr.*, **12**, 1169–1188, doi:10.1175/1520-0485(1982)012<1169:TSMWOT>2.0.CO;2.

——, S. L. Bennett, and M. E. Woodgate-Jones, 1991: Eastward flow through the Mid-Atlantic Ridge at 11°N and its influence on the abyss of the eastern basin. *J. Phys. Oceanogr.*, **21**, 1089–1121, doi:10.1175/1520-0485(1991)021<1089:EFTTMA>2.0.CO;2.

Ochoa, J., and N. A. Bray, 1991: Water mass exchange in the Gulf of Cadiz. *Deep-Sea Res.*, **38A**, S465–S503, doi:10.1016/S0198-0149(12)80021-5.

Paillet, J., and M. Arhan, 1996: Oceanic ventilation in the eastern North Atlantic. *J. Phys. Oceanogr.*, **26**, 2036–2052, doi:10.1175/1520-0485(1996)026<2036:OVITEN>2.0.CO;2.

——, and H. Mercier, 1997: An inverse model of the eastern North Atlantic general circulation and thermocline ventilation. *Deep-Sea Res. I*, **44**, 1293–1328, doi:10.1016/S0967-0637(97)00019-8.

——, M. Arhan, and M. S. McCartney, 1998: Spreading of Labrador Sea Water in the eastern North Atlantic. *J. Geophys. Res.*, **103**, 10 223–10 239, doi:10.1029/98JC00262.

Pardo, P. C., F. F. Pérez, A. Velo, and M. Gilcoto, 2012: Water masses distribution in the Southern Ocean: Improvement of an extended OMP (eOMP) analysis. *Prog. Oceanogr.*, **103**, 92–105, doi:10.1016/j.pocean.2012.06.002.

Pérez, F. F., C. Mouriño, F. Fraga, and A. F. Rios, 1993: Displacement of water masses and remineralization rates off the Iberian Peninsula by nutrient anomalies. *J. Mar. Res.*, **51**, 869–892, doi:10.1357/0022240933223891.

——, A. F. Rìos, C. G. Castro, and F. Fraga, 1998: Mixing analysis of nutrients, oxygen and dissolved inorganic carbon in the upper and middle North Atlantic Ocean east of the Azores. *J. Mar. Syst.*, **16**, 219–233, doi:10.1016/S0924-7963(97)00108-5.

——, and Coauthors, 2001: Mixing analysis of nutrients, oxygen and inorganic carbon in the Canary Islands region. *J. Mar. Syst.*, **28**, 183–201, doi:10.1016/S0924-7963(01)00003-3.

Pollard, R. T., and S. Pu, 1985: Structure and circulation of the upper Atlantic Ocean northeast of the Azores. *Prog. Oceanogr.*, **14**, 443–462, doi:10.1016/0079-6611(85)90022-9.

Poole, R., and M. Tomczak, 1999: Optimum multiparameter analysis of the water mass structure in the Atlantic Ocean thermocline. *Deep-Sea Res. I*, **46**, 1895–1921, doi:10.1016/S0967-0637(99)00025-4.

Price, J. F., and Coauthors, 1993: Mediterranean outflow mixing and dynamics. *Science*, **259**, 1277–1282, doi:10.1126/science.259.5099.1277.

Reid, J. L., 1978: On the middepth circulation and salinity field in the North Atlantic Ocean. *J. Geophys. Res.*, **83**, 5063–5067, doi:10.1029/JC083iC10p05063.

——, 1979: On the contribution of the Mediterranean Sea outflow to the Norwegian-Greenland Sea. *Deep-Sea Res.*, **26A**, 1199–1223, doi:10.1016/0198-0149(79)90064-5.

——, 1994: On the total geostrophic circulation of the North Atlantic Ocean: Flow patterns, tracers, and transports. *Prog. Oceanogr.*, **33**, 1–92, doi:10.1016/0079-6611(94)90014-0.

Rhein, M., and H. H. Hinrichsen, 1993: Modification of Mediterranean Water in the Gulf of Cadiz, studied with hydrographic, nutrient and chlorofluoromethane data. *Deep-Sea Res. I*, **40**, 267–291, doi:10.1016/0967-0637(93)90004-M.

Ríos, A. F., F. F. Pérez, and F. Fraga, 1992: Water masses in the upper and middle North Atlantic Ocean east of the Azores. *Deep-Sea Res.*, **39A**, 645–658, doi:10.1016/0198-0149(92)90093-9.

Sannino, G., L. Pratt, and A. Carillo, 2009: Hydraulic criticality of the exchange flow through the Strait of Gibraltar. *J. Phys. Oceanogr.*, **39**, 2779–2799, doi:10.1175/2009JPO4075.1.

Saunders, P. M., 1982: Circulation in the eastern North Atlantic. *J. Mar. Res.*, **40**, 641–657.

Schmitz, W. J., Jr., 1996: On the World Ocean circulation: Volume I. Some global features/North Atlantic circulation. Woods Hole Oceanographic Institution Tech. Rep. WHOI-96-03, 148 pp.

Shapiro, G. I., and S. L. Meschanov, 1996: Spreading pattern and mesoscale structure of Mediterranean outflow in the Iberian basin estimated from historical data. *J. Mar. Syst.*, **7**, 337–348, doi:10.1016/0924-7963(95)00011-9.

Siedler, G., J. Church, and J. Gould, Eds., 2001: *Ocean Circulation and Climate: Observing and Modelling the Global Ocean*. Academic Press, 715 pp.

Talley, L. D., 1996: Antarctic Intermediate Water in the South Atlantic. *The South Atlantic: Present and Past Circulation*, G. Wefer et al., Eds., Springer-Verlag, 219–238.

Tomczak, M., 1981: A multi-parameter extension of temperature/salinity diagram techniques for the analysis of non-isopycnal mixing. *Prog. Oceanogr.*, **10**, 147–171, doi:10.1016/0079-6611(81)90010-0.

——, and P. Hughes, 1980: Three-dimensional variability of water masses and currents in the Canary Current upwelling region. *''Meteor'' Forschungsergeb.*, **A21**, 1–24.

——, and D. G. B. Large, 1989: Optimum multiparameter analysis of mixing in the thermocline of the eastern Indian Ocean. *J. Geophys. Res.*, **94**, 16 141–16 149, doi:10.1029/JC094iC11p16141.

Tsuchiya, M., 1989: Circulation of the Antarctic Intermediate Water in the North Atlantic Ocean. *J. Mar. Res.*, **47**, 747–755, doi:10.1357/002224089785076136.

——, L. D. Talley, and M. S. McCartney, 1992: An eastern Atlantic section from Iceland southward across the equator. *Deep-Sea Res.*, **39A**, 1885–1917, doi:10.1016/0198-0149(92)90004-D.

van Aken, H. M., 2000a: The hydrography of the mid-latitude northeast Atlantic Ocean: I: The deep water masses. *Deep-Sea Res. I*, **47**, 757–788, doi:10.1016/S0967-0637(99)00092-8.

——, 2000b: The hydrography of the mid-latitude Northeast Atlantic Ocean: II: The intermediate water masses. *Deep-Sea Res. I*, **47**, 789–824, doi:10.1016/S0967-0637(99)00112-0.

Weiss, R. F., 1970: The solubility of nitrogen, oxygen and argon in water and seawater. *Deep-Sea Res. Oceanogr. Abstr.*, **17**, 721–735, doi:10.1016/0011-7471(70)90037-9.

Worthington, L. V., 1976: *On the North Atlantic Circulation.* Johns Hopkins University Press, 110 pp.

Zenk, W., 1970: On the temperature and salinity structure of the Mediterranean Water in the northeast Atlantic. *Deep-Sea Res. Oceanogr. Abstr.*, **17**, 627–631, doi:10.1016/0011-7471(70)90072-0.

——, 1975: On the Mediterranean outflow west of Gibraltar. *''Meteor'' Forschungsergeb.*, **16**, 23–24.

——, and L. Armi, 1990: The complex spreading pattern of Mediterranean Water off the Portuguese continental slope. *Deep-Sea Res.*, **37A**, 1805–1823, doi:10.1016/0198-0149(90)90079-B.